# Effects of bulk and wall chemical reactions on hydrodynamic dispersion of a solute in a couple stress fluid

Radha S [1], Swarup Barik [1,*,†] and Nanda Poddar [2,‡]
[1]*Department of Mathematics, College of Engineering and Technology, SRM Institute of Science and Technology, Kattankulathur, Tamilnadu 603203, India*
[2]*School of Mathematical and Statistical Science, University of Galway, Galway H91TK33, Ireland*

(Received 20 May 2024; accepted 3 January 2025; published 29 January 2025)

This paper presents an analytical exploration of the two-dimensional concentration distribution of a solute under the influence of first-order bulk and wall chemical reactions in a viscous, couple stress fluid flowing between two parallel plates. The analytical expressions for mean and transverse concentration distributions up to third order are derived using Mei and Vernescu's multiscale homogenization technique. This paper meticulously investigates the impact of a couple stress parameter ($\alpha$) and the chemical reaction parameters on Taylor dispersion through a reactive solute's dispersion coefficient, mean, and transverse concentration distributions. Results reveal that the effect of couple stress is most significant for smaller values of $\alpha$ (i.e., $20 > \alpha \geqslant 1$), in which the dispersion increases and the tracer particle's mean concentration decreases. As $\alpha$ increases, there is a decreasing trend in dispersion, and for a large value of $\alpha$ a subtle decrease in dispersion is observed, which implies that the increment in viscosity impacts the dispersion coefficient. However, the negligible effect of couple stress ($\alpha \gg 20$) results in a subtle increase in the mean concentration distribution. Increasing the value of the bulk chemical reaction parameter uniformly decreases the transverse concentration more effectively for smaller values of $\alpha$. Both couple stress and wall reactions significantly impact the concentration variation by inducing nonuniformity. Interestingly, at the center of the channel cross section, the bulk chemical reaction is more efficient in decreasing the transverse concentration profile when compared to wall chemical reactions, especially for smaller values of $\alpha$ where the couple stress is notably high. The results are effective as they are pivotal in advancing the design and performance of microfluidic devices, enhancing the separation of fluids and components, and improving fluid mixing efficiency.

DOI: 10.1103/PhysRevFluids.10.014502

## I. INTRODUCTION

Exploring and modeling complex fluid systems play a critical role in many industries, such as shaping the design and development of cutting-edge technologies, which include innovations like microfluidic devices, laboratory-on-a-chip platforms, and advanced materials [1–3]. Many applications, both in industry [4] and the scientific realm [5], deal with intricate fluid dynamics, often characterized by the significant impact of couple stress [6]. Modeling these kinds of systems

*Contact author: swarupb@srmist.edu.in
†Also at Department of Civil Engineering, National Taiwan University, Taipei 10617, Taiwan.
‡Also at Department of Environmental Physics, BIDR, Ben-Gurion University of the Negev, Sde Boker 8499000, Israel.

 

is necessary to predict and optimize the performance of systems and processes in their applications. The dispersion of solutes within these systems is influenced by multiple factors, including the physical, chemical, and mechanical properties of the materials involved, the position of solute sources, and the surrounding environment. By applying fundamental principles like Fick's law, we can develop mathematical models to describe the distribution of solute concentrations resulting from these materials. Several dispersion models have been developed to study this phenomenon, each with its characteristics. One such longstanding work is Taylor's [7] dispersion, which explored the dispersion of soluble substances within a tube and introduced the concept of shear stress. The author noted that the varying velocity shear along the direction of flow results in increased solute diffusion. Building upon Taylor's work, Aris [8] further expanded the research, eliminating the constraints Taylor set and incorporating longitudinal dispersion into Taylor's findings, introducing the moment method to analyze the convection process. Gill and Sankarasubramanian [9] introduced a technique based on series expansion to address convective diffusion problems accurately. They also determined an average concentration distribution that covers a wide range of independent variable values for a one-dimensional dispersion model. Chatwin [10] presented a method for attaining longitudinal normality in mean concentration, which involved the development of an asymptotic series for the concentration distribution, with the constraint that solute diffusion adheres to Fick's law. Barton [11] examined the dispersion process in pipes or channels, formulated an eigenvalue problem, and effectively tackled technical challenges related to the Aris technique of moments. As a result, Barton provided comprehensive solutions for the second- and third-moment equations that govern solute distribution and reexamined the outcomes of Chatwin's research. Wang and Chen [12] investigated how a solute initially disperses within a laminar flow tube and observed a distinctive saddle-shaped concentration profile developing in the tube's center, attributed to differences in flow velocity.

The concept of couple stresses is an extension of classical fluid mechanics that considers the influence of internal rotational moments, or couple stresses, in addition to the traditional stresses associated with fluid pressure and viscosity. Couple stresses can significantly describe the behavior of certain complex fluids, such as non-Newtonian fluids, microscale and nanoscale fluids, or fluids with suspended particles. Stokes [13] introduced the theory of couple stress fluids, which belongs to the category of polar non-Newtonian fluid theories, and expands upon the traditional understanding of viscous fluid dynamics, which typically focuses on classical Cauchy stresses. It provides the most straightforward framework for developing a conventional fluid theory to account for polar effects, notably including couple stresses and body couples. Couple stress theory provides an accurate description of how fluids with inherent structures, such as lubricants with long-chain molecules, liquid crystals, suspensions of nanoparticles, emulsions of oil and water, and animal blood, behave in terms of their flow [14,15]. This research has gained prominence due to the influence of such fluids in chemical engineering, including applications that encompass the utilization of these fluids in a range of scenarios, such as incorporating them in polymer-thickened oils, deploying them in the context of liquid crystals, exploring their relevance in physiological fluid mechanics [16], and employing them in polymeric suspensions [17]. The effect of couple stress on dispersion is essential for advancing scientific knowledge, fostering innovation, solving real-world problems, and optimizing operations [18,19]. It has far-reaching implications in fields ranging from engineering and environmental science to health and safety, making it a valuable study area in scientific research. Soundalgekar's [20] work sheds light on how the presence of couple stress, a measure of the internal stresses within a fluid, can influence the process of dispersion and its associated coefficient. Later, he delved into the impact of couple stress and various chemical reactions on solute dispersion. The findings revealed that couple stress is more pronounced in homogeneous reactions at lower $\alpha$ values, while its influence diminishes as $\alpha$ increases. Conversely, in the case of inhomogeneous reactions, dispersion experiences a notable increase, indicating an enhanced solute dispersion effect [21,22]. Later, Rudraiah *et al.* [23] examined the influence of couple stress on an unsteady convective diffusion in fluid flow through a channel. Their results explore that the couple stress plays a significant role for smaller values of $\alpha$, and as $\alpha$ approaches infinity, the flow behavior tends to

resemble that of Newtonian theory. Additionally, their findings demonstrate the recovery of Taylor's dispersion model as a specific case in the limit where $\tau \to \infty$.

In chemical engineering, understanding solute dispersion is crucial for optimizing various processes. Especially in many chemical engineering problems, irreversible first-order chemical reactions occur, leading to solute diffusion happening simultaneously with these reactions. Researchers have analyzed the dispersion problem by incorporating first-order bulk chemical reactions under laminar flow to depict these situations accurately. Furthermore, if the channel wall is catalytic, wall chemical reactions at the surface can arise, adding another layer of complexity to the dispersion process. Katz [24] explored this phenomenon, emphasizing the influence of catalyzed wall chemical reactions on the tube wall. Walker [25] offered a general solution to address the axially symmetric problems associated with diffusion, convection, and reaction of a reactant within a catalytic tubular reactor. His investigation also included an analysis of the reactant's decay both upstream and downstream of the source. Researchers like Gupta and Gupta [26], Neely *et al.* [27], Philip and Chandra [28], along with many others, have extensively studied the combined impacts of bulk chemical and wall chemical reactions in dispersing solutes within Newtonian fluid flow. This paper incorporates both first-order bulk and wall chemical reactions along with the effect of couple stress. Ng and Rudraiah [29] analyzed mass transport in steady Poiseuille flow through a circular tube with reactive walls, combining reversible and irreversible reactions. They derived steady-state transport coefficients using a dispersion model and simulated time-dependent concentration profiles to explain trends in transport behavior. Debnath *et al.* [30] studied solute dispersion in an annular pipe under a periodic pressure gradient. They found that in a steady flow, the dispersion coefficient quickly stabilizes at high reaction rates, with the bulk flow reaction parameter having less impact. Roy *et al.* [31] studied Taylor dispersion of reactive species in Casson liquid under oscillatory flow, with solute reactions at the boundary and in the bulk. They found that wall absorption and bulk flow reactions affect dispersion by reducing the negative exchange coefficient and increasing the negative convection coefficient. Jiang and Chen [32] developed a simplified analytical model to investigate reactive transport involving boundary adsorption and desorption. They analyzed various concentration distributions, including bulk, surface, transverse average, and overall mean concentrations. Recently, Saha *et al.* [33] investigated the effect of the Grashof number in the presence of bulk and wall chemical reactions and found that Taylor dispersivity is equal for both the positive and negative Grashof number, i.e., for heating and cooling respectively. Also, the longitudinal concentration of solute decreases when both the cooling and heating processes increase. Poddar *et al.* [34] delved into the investigation of solute transport in an oscillatory Couette-Poiseuille flow between two parallel plates in the presence of bulk chemical and wall chemical reactions. Their results reveal that with boundary absorption, the concentration profile fluctuates most rapidly along the upstream and downstream directions, respectively, for steady and moving plates.

This paper delves into the transverse concentration distribution of viscous flow with a couple stress effect, encompassing the influence of chemical reactions by utilizing the multiscale framework of Mei and Vernescu [35]. This framework seeks to build accurate macroscale models by averaging over the swift fluctuations of fast variables, thus bypassing the limitations of traditional one-scale approaches, which stumble on both macrolevel accuracy and microlevel efficacy. The primary objective of employing the multiscale method is to individually capture the effects of different physical processes. Specifically, lateral diffusion, advection, and longitudinal diffusion can occur simultaneously, each with its own characteristic timescale. For instance, in a narrow geometry, diffusion in the lateral direction happens quickly, necessitating the assignment of a short timescale to account for these rapid variations. In contrast, advection is slower than lateral diffusion, and longitudinal diffusion occurs even more slowly. Consequently, we assign medium and long timescales for advection and longitudinal diffusion, respectively. This distinction is a key difference between the multiscale method and single-time-scale methods, such as those proposed by Aris and Gill. Another advantage of the multiscale technique is its ability to simultaneously evaluate the dispersion coefficient, mean concentration distribution, and two-dimensional concentration distribution. In recent times, transverse concentration has become essential because of its applications in various

industries. The present paper sheds light on the transverse concentration distribution, revealing the intricate relation between solutes and flow dynamics across the entire flow field. Previous research primarily focused on the mean concentration, neglecting the crucial variations across the flow cross section. The pioneering research of Ng [36,37] becomes important in studying transverse distribution by examining sorption with the bed and air-water reactions in tubes and open channels, both under steady and oscillating flows. Wu and Chen [38,39] were among the first to delve into the nonuniformity of transverse concentration in laminar flows, revealing a slower transverse uniformity compared with longitudinal uniformity. Importantly, they proposed a timescale for assessing the uniformity in both upstream and downstream regions. Barik and Dalal [40] utilized a multiscale approach to investigate the impact of bed absorption on transverse distribution in open channels, highlighting the significant nonuniformity it induces, especially downstream. Poddar *et al.* [41,42] and Dhar *et al.* [43] further explored transverse distribution under the influence of magnetic fields and boundary absorption in parallel plate flows, emphasizing the substantial nonuniformity caused by these factors. Karmakar *et al.* [44] revealed how contaminant dispersion, pressure pulsations, and wall oscillations interact in a fluid between porous plates, finding that pulse frequency affects dispersion significantly, while wall oscillations dominate when the Womersley number is constant. Recent advancements in solute transport research have utilized the multiscale homogenization technique across various flow fields, extending earlier foundational work. Poddar and Wang [45] applied this method to analyze dispersion and concentration distributions in wetland beds, incorporating vegetation effects and surface reactions. They further extended Ng and Yip's [46] work by including magnetic fields and boundary absorption [47], refining the understanding of solute transport. Wang *et al.* [48] recently demonstrated that balanced absorptive beds in constructed wetlands improve contaminant removal efficiency by up to 30%. Recently, researchers [49–51] have predominantly utilized multiscale homogenization method to examine the solute transport phenomena in Newtonian and non-Newtonian flows influenced by irreversible boundary reactions. These studies underscore the versatility and effectiveness of multiscale homogenization in advancing solute transport modeling.

The present paper introduces an investigation into the intricate interplay between couple stress and various chemical reaction parameters; while previous research has explored the individual effects, very few studies have systematically studied their combined impacts on dispersion phenomena [22]. Our paper fills this gap by conducting a comprehensive comparative analysis, elucidating the enigmatic relationships between couple stress and various chemical reaction parameters on mean and transverse concentration distributions. This paper delineates the distinct influences of each chemical reaction and couple stress parameters, expounding their respective contributions to the overall system behavior. Also, this research underscores its vital importance in shedding light on these phenomena, highlighting its considerable importance in advancing the solute transport dynamics. We aim to unravel the intricate effects of couple stress alongside diverse chemical reactions. In this paper, we utilized the multiscale method to derive analytical solutions for the mean and transverse concentration distributions in viscous fluids to delve into the effect of couple stress and various chemical reactions. The paramount aim of this research is to unravel post-transient behavior, wherein we endeavor to determine the mean and two-dimensional concentration distribution in viscous fluids with the couple stress effect. The significant necessity of this research is due to its real-time applications, particularly in domains of microfluidic devices and pollutant degradation where the combined effect of couple stress and chemical reactions holds immense promise. This paper investigates the influence of couple stress on the channel flow and the transitional evolution of the concentration distribution. This investigation delves into how bulk and wall chemical reactions influence solute dispersion in flow and transverse directions. This paper also examines the transverse uniformity and nonuniformity of the concentration cloud caused by the couple stress, bulk chemical, and wall chemical reactions parameters, respectively. The precise goals of this investigation are to delve into a better understanding of complex microstructure systems and the solute transport phenomena on such systems.

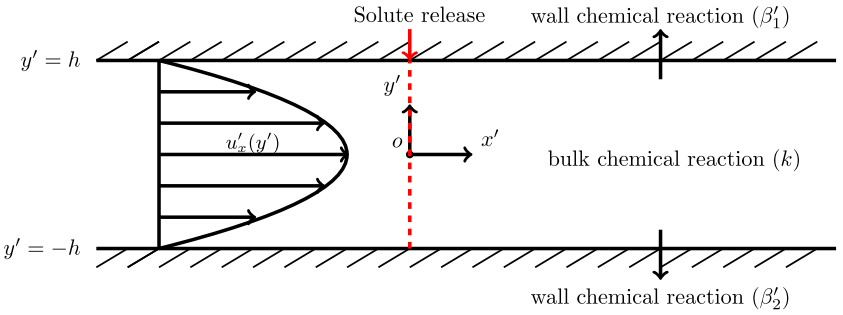


FIG. 1. Sketch for the instantaneous release of solute (red color) between parallel plates with absorbing boundaries.

The framework of this paper and its several significant aspects are outlined as follows: Sec. II deals with the formulation of the problem mathematically, followed by the dimensionalization of the governing equations and velocity profile. The analytical methodology to derive the solution of the expressions for the significant flow quantities, such as dispersion coefficient, mean, and two-dimensional transverse concentration distribution of the solute, is presented in Sec. III. In Sec. IV, the numerical simulation is performed to explore further and validate the analytical results, providing additional insights into the system's behavior. The impacts of full implication of various parameters such as couple stress parameter, wall, and bulk chemical reaction parameters on the above flow quantities are analyzed visually through graphs, and the distinct combination of various parameters and their characteristic behavior in all possible scenarios of the flow quantities are discussed in detail in Sec. V. The applications of the present paper are presented in Sec. VI. The results and observations of the investigation are summarized as points in the concluding Sec. VII.

## II. MATHEMATICAL FORMULATION OF THE PROBLEM

Consider a fully developed, laminar, unidirectional flow of a viscous couple stress fluid between two parallel plates separated by a distance of $2h$. A Cartesian coordinate system $ox'y'$ has been employed, with $x'$ signifying the horizontal coordinate axis, $y'$ representing the coordinate axis perpendicular to the flow, and the origin $o$ being situated at the center of the channel. The channel plates are established along the lines $y' = \pm h$ (see Fig. 1). Both plates are considered stationary, and the flow results from a constant pressure gradient in the positive $x'$ direction. For the flow of a Newtonian fluid in the presence of couple stress, the momentum equation in the $x'$ direction is as follows [13]:

$$0 = -\frac{\partial p}{\partial x'} + \mu \frac{\partial^2 u_x'}{\partial y'^2} - \eta \frac{\partial^4 u_x'}{\partial y'^4}, \tag{1}$$

where $u_x'$ signifies the velocity in the $x'$ direction, $p$ is the pressure, $\frac{\partial p}{\partial x'}$ is the pressure gradient along the plates, $\mu$ is the dynamic viscosity, and $\eta$ is a material constant which is associated with the couple stress. The term $\eta \frac{\partial^4 u_x'}{\partial y'^4}$ reflects the impact of couple stress by incorporating higher-order spatial derivatives into the momentum equation. This inclusion captures the additional complexities introduced by couple stress, which are not present in classical Newtonian fluids characterized only by first-order viscosity effects. In other words, couple stress modifies the classical stress-strain relationship by adding these higher-order terms. This modification accounts for additional forces and influences within the fluid that result from its microstructural properties, such as the interactions between fluid elements. Such effects become significant in fluids where these microstructural interactions cannot be ignored.

Using Eq. (1), the equation that governs this flow of incompressible fluid with couple stress is as follows:

$$\frac{d^4u_x'}{dy'^4} - \frac{1}{l^2}\frac{d^2u_x'}{dy'^2} + \frac{1}{\eta}\frac{\partial p}{\partial x'} = 0, \tag{2}$$

where $l^2 = \eta/\mu$ refers to the material constant with the dimension of length squared, which characterizes the influence of couple stress.

Subject to the no-slip boundary conditions

$$u_x'(y') = 0, \quad \text{at} \quad y' = \pm h, \tag{3}$$

the expression of the flow velocity is derived as [13]

$$u_x'(y') = U\left[1 - \left(\frac{y'}{h}\right)^2 - \frac{2l^2}{h^2}\left\{1 - \frac{\cosh(y'/l)}{\cosh(h/l)}\right\}\right], \tag{4}$$

where $U(= \frac{1}{2}\frac{\partial p}{\partial x'}\frac{h^2}{\mu})$ is the reference velocity.

When a solute with a constant diffusion coefficient $D$ is introduced into the flowing fluid, the governing equation of the transport of the solute is of the form

$$\frac{\partial C'}{\partial t'} + u_x'(y')\frac{\partial C'}{\partial x'} = D\left(\frac{\partial^2 C'}{\partial x'^2} + \frac{\partial^2 C'}{\partial y'^2}\right) - kC', \quad -h < y' < h, \tag{5}$$

where $C'(x', y', t')$ is the solute concentration and $k$ represents the dimensional first-order bulk chemical reaction parameter, which defines the reaction rate within the fluid flow and affects solute concentration throughout the channel, such as in chemical processing or reactor systems.

The solute undergoes an irreversible chemical reaction at both channel plates, and the initial and boundary conditions for the above flow are as follows [21,52]:

$$C'(x', y', t')|_{t'=0} = \frac{m_s}{h}\delta\left(\frac{x'}{h}\right), \tag{6}$$

$$D\frac{\partial C'(x', y', t')}{\partial y'}\bigg|_{y'=-h} = \beta_2' C'(x', -h, t'), \tag{7}$$

$$D\frac{\partial C'(x', y', t')}{\partial y'}\bigg|_{y'=h} = -\beta_1' C'(x', h, t'), \tag{8}$$

where $m_s$ is the mass of the solute released uniformly across the width at time $t' = 0$. Here, $\delta(x'/h)$ denotes the Dirac delta function, and $\beta_1'$ and $\beta_2'$ denote the chemical reaction rate parameters at the channel plates that regulate the chemical interactions between the solute and the plates. These reactions may lead to the absorption of the reacted solute by the channel plates. Since the injected solute is of finite quantity, it is also assumed that, at large upstream and downstream distances, the concentration of the tracers becomes negligible, i.e.,

$$C'(x', y', t')|_{x'\to\pm\infty} = 0. \tag{9}$$

## III. MULTISCALE METHOD OF HOMOGENIZATION

### A. Scale selection

In this paper, we utilize Mei and Vernescu's homogenization method [35] to perform asymptotic analysis. We consider two distinct length scales: $h$, representing half of the channel width, and $L$, signifying the characteristic longitudinal length of the channel. Furthermore, we introduced three distinct timescales for different transport processes: The short timescale $T_0$ corresponds to the time for diffusion along the lateral direction and can be expressed as $T_0 = h^2/D$. The medium timescale $T_1$ represents the time for advection across the characteristic length $L$ and is defined as $T_1 = L/\langle u_x'\rangle$.

The long timescale $T_2$ characterizes the time for diffusion along the flow direction and can be calculated as $T_2 = L^2/D$. Furthermore, the ratios between these timescales introduced by Mei and Vernescu can be written as

$$T_0 : T_1 : T_2 = 1 : \frac{1}{\epsilon} : \frac{1}{\epsilon^2}, \tag{10}$$

where $\epsilon$ $(= h/L \ll 1)$ is considered as the perturbation parameter and

$$\langle u_x' \rangle = \frac{1}{2h} \int_{-h}^{h} u_x' dy \tag{11}$$

is the transverse mean of the velocity $u_x'$.

### B. Dimensionless form of the governing equation and the velocity profile

Introducing the dimensionless parameters as

$$x = \frac{x'}{L}, \quad y = \frac{y'}{h}, \quad u_x = \frac{u_x'}{\langle u_x' \rangle}, \quad t = \frac{t'}{h^2/D}, \quad C = \frac{C'}{m_s/h}, \quad \mathrm{Pe} = \frac{\langle u_x' \rangle h}{D},$$
$$\beta_1 = \frac{\beta_1' L}{D}, \quad \beta_2 = \frac{\beta_2' L}{D}, \quad K = \frac{kL^2}{D}, \tag{12}$$

where Pe is the Péclet number, which can be determined as the ratio of the advection rate ($\frac{1}{h/\langle u_x' \rangle}$) to the diffusion rate ($\frac{1}{h^2/D}$), and $\beta_1$ and $\beta_2$ are the dimensionless wall chemical reaction rate parameters along the parallel plates.

Using the corresponding dimensionless forms of Eqs. (5)–(9), the governing equation, initial conditions, and boundary conditions are rewritten as

$$\frac{\partial C}{\partial t} + \epsilon \,\mathrm{Pe}\, u_x \frac{\partial C}{\partial x} = \epsilon^2 \frac{\partial^2 C}{\partial x^2} + \frac{\partial^2 C}{\partial y^2} - \epsilon^2 K C, \quad -1 < y < 1, \tag{13}$$

$$C(x, y, t)|_{t=0} = \delta\left(\frac{x}{\epsilon}\right), \tag{14}$$

$$\left.\frac{\partial C(x, y, t)}{\partial y}\right|_{y=-1} = \epsilon \beta_2 C(x, -1, t), \tag{15}$$

$$\left.\frac{\partial C(x, y, t)}{\partial y}\right|_{y=1} = -\epsilon \beta_1 C(x, 1, t), \tag{16}$$

$$C(x, y, t)|_{x=\pm\infty} = 0. \tag{17}$$

The dimensionless velocity profile for the channel flow is given as

$$u_x(y) = \frac{1 - y^2 - \frac{2}{\alpha^2}\left(1 - \frac{\cosh(\alpha y)}{\cosh \alpha}\right)}{\frac{2}{3} - \frac{2}{\alpha^2}\left(1 - \frac{\tanh \alpha}{\alpha}\right)}, \tag{18}$$

where

$$\alpha = \frac{h}{l} \tag{19}$$

is the couple stress parameter, with $l = \sqrt{\frac{\eta}{\mu}}$ a material constant representing the length scale related to fluids microstructure. Here, the couple stress parameter $\alpha$ plays a crucial role in governing the fluid flow behavior since it considers the presence of microrotations and internal couple moments within the fluid. However, the large $\alpha$ indicates a weak couple stress effect while the small $\alpha$ value indicates a strong couple stress effect. These couple stresses emerge from the rotation of fluid elements, which creates additional stress within the fluid. In other words, as $\alpha$ increases, the

couple stress effect becomes negligible because the rotational effects do not significantly impact the overall flow, whereas when $\alpha$ decreases, the couple stress effect becomes dominant, i.e., the internal rotation of the fluid element causes the fluid element to resist shear more effectively. In Eq. (18), as $\alpha \to \infty$ the equation simplifies to $\frac{3}{2}(1 - y^2)$ [20,23], which corresponds to the classical parabolic velocity distribution observed in plane Poiseuille flow, indicating that the flow is dominated by viscous effect in the absence of couple stress (i.e., $\alpha \to \infty$). In contrast, when $\alpha \not\to \infty$, Eq. (18) signifies the modifications due to couple stress, reflecting how these effects alter the velocity profile compared to the classical case. This parameter $\alpha$ illustrates the impact of couple stress on the flow, highlighting deviations from the classical profile. Therefore, varying $\alpha$ influences the couple stress on the velocity distribution and ensures the profile remains consistent with the physical constraints of the flow. Moreover, by choosing appropriate values of $\alpha$, one can effectively control the flow; this is analogous to controlling flow properties in fluids with large molecular structures, such as polymers, where the length of the polymer chains plays a critical role in determining the couple stress influence on the flow dynamics [53].

### C. Asymptotic analysis: Homogenization

The homogenization technique of Mei and Vernescu [35](see also [54]) is utilized for asymptotic analysis. Expand the concentration $C$ asymptotically in multiple scales as [10,40,55]

$$C(x, y, t) = C^{(0)}(x, y, t_0, t_1, t_2) + \epsilon C^{(1)}(x, y, t_0, t_1, t_2) + \epsilon^2 C^{(2)}(x, y, t_0, t_1, t_2) + \epsilon^3 C^{(3)}(x, y, t_0, t_1, t_2) + O(\epsilon^4), \tag{20}$$

where $C^{(0)}, C^{(1)}, C^{(2)}$, and $C^{(3)}$ correspond to concentration distributions of zeroth, first, second, and third orders, while $O(\epsilon^4)$ accounts for higher-order terms. Here, $C^{(0)}$ is the dominant term that represents the concentration at the leading order and $C^{(1)}$, $C^{(2)}$, and $C^{(3)}$ are known as the correction terms to the leading-order solution.

Based on the three timescales defined earlier, we have introduced fast ($t_0$), medium ($t_1$), and slow ($t_2$) time variables as follows [35]:

$$t_0 = t, \quad t_1 = \epsilon t, \quad t_2 = \epsilon^2 t. \tag{21}$$

Here, different time variables are introduced to effectively separate and analyze the dynamics of processes occurring at varying rates. The fast time variable $t_0$, designated as the original time variable $t$, will account for the rapid variations induced by lateral diffusion within the short timescale $T_0$. The medium time variable $t_1$ evolves at a slower rate, specifically by a factor of $\epsilon$, and will capture the relatively slow behavior advection in the defined timescale $T_1$. In contrast, the slow time variable $t_2$ $(= \epsilon^2 t)$ captures the slowest behavior of the diffusion process occurring in the longitudinal direction over the long timescale $T_2$.

Using the chain rule, the original time derivatives are obtained as

$$\frac{\partial}{\partial t} = \frac{\partial}{\partial t_0} + \epsilon \frac{\partial}{\partial t_1} + \epsilon^2 \frac{\partial}{\partial t_2}. \tag{22}$$

On applying Eqs. (20) and (22) in Eqs. (13), (15), and (16), we can deduce the following for zeroth-order perturbation [$O(1)$]:

$$\frac{\partial C^{(0)}}{\partial t_0} = \frac{\partial^2 C^{(0)}}{\partial y^2}, \quad -1 < y < 1, \tag{23}$$

and

$$\left.\frac{\partial C^{(0)}}{\partial y}\right|_{y=-1} = \left.\frac{\partial C^{(0)}}{\partial y}\right|_{y=1} = 0. \tag{24}$$

Using the boundary conditions of Eq. (24), the general solution of Eq. (23) is as follows:

$$C^{(0)} = C_0^{(0)}(x, t_1, t_2) + \sum_{n=1}^{\infty} \mathrm{Re}\left[C_n^{(0)}(x, t_1, t_2) e^{in\pi y}\right] e^{-n^2\pi^2 t_0}. \tag{25}$$

Due to the rapid exponential decay of the series term [35], Eq. (25) transforms into the following form:

$$C^{(0)} = C^{(0)}(x, t_1, t_2). \tag{26}$$

We obtain the first-order $O(\epsilon)$ perturbation from Eqs. (13)–(16) and (20)–(22):

$$\frac{\partial C^{(0)}}{\partial t_1} + \frac{\partial C^{(1)}}{\partial t_0} + \mathrm{Pe}\, u_x \frac{\partial C^{(0)}}{\partial x} = \frac{\partial^2 C^{(1)}}{\partial y^2}, \quad -1 < y < 1, \tag{27}$$

and

$$\left(\frac{\partial C^{(1)}}{\partial y} - \beta_2 C^{(0)}\right)\Big|_{y=-1} = 0, \quad \left(\frac{\partial C^{(1)}}{\partial y} + \beta_1 C^{(0)}\right)\Big|_{y=1} = 0. \tag{28}$$

The left-hand side of the second term in Eq. (27), characterized by a significantly larger time variable of $t_0$ compared to $t_1$, can be neglected:

$$\frac{\partial C^{(0)}}{\partial t_1} + \mathrm{Pe}\, u_x \frac{\partial C^{(0)}}{\partial x} = \frac{\partial^2 C^{(1)}}{\partial y^2}, \quad -1 < y < 1. \tag{29}$$

Moreover, considering the spatial variable $y$ and the boundary conditions in Eqs. (28), we can determine the sectional average of Eq. (29) as

$$\frac{\partial C^{(0)}}{\partial t_1} + \mathrm{Pe}\langle u_x\rangle \frac{\partial C^{(0)}}{\partial x} = -\frac{1}{2}(\beta_1 + \beta_2) C^{(0)}, \quad -1 < y < 1. \tag{30}$$

Utilizing Eqs. (29) and (30) we obtain

$$\mathrm{Pe}\,(u_x - \langle u_x\rangle)\frac{\partial C^{(0)}}{\partial x} - \frac{1}{2}(\beta_1 + \beta_2) C^{(0)} = \frac{\partial^2 C^{(1)}}{\partial y^2}, \quad -1 < y < 1. \tag{31}$$

The above equation suggests the following ansatz to express the higher-order terms in terms of the leading-order solutions:

$$C^{(1)} = \mathrm{Pe}\, N(y) \frac{\partial C^{(0)}}{\partial x} + \frac{1}{2}(\beta_1 + \beta_2) M(y) C^{(0)}, \tag{32}$$

where the coefficients $N(y)$ and $M(y)$ are determined by eliminating $C^{(1)}$ from Eqs. (31), (32), and (28). The function $N(y)$ will be governed by

$$\frac{d^2 N}{dy^2} = u_x - \langle u_x\rangle, \quad -1 < y < 1, \tag{33}$$

with the boundary conditions

$$\frac{dN}{dy}\Big|_{y=-1} = \frac{dN}{dy}\Big|_{y=1} = 0, \tag{34}$$

and

$$\langle N\rangle = 0. \tag{35}$$

Again, $M(y)$ satisfies the following equations:

$$\frac{d^2 M}{dy^2} = -1, \quad -1 < y < 1, \tag{36}$$

with the boundary conditions

$$\left.\frac{dM}{dy}\right|_{y=-1} = \frac{2\beta_2}{\beta_1+\beta_2}, \quad \left.\frac{dM}{dy}\right|_{y=1} = \frac{-2\beta_1}{\beta_1+\beta_2}, \tag{37}$$

and

$$\langle M\rangle = 0. \tag{38}$$

On solving Eqs. (33)–(38), one can determine

$$N(y) = \frac{1}{120\alpha^2[(\alpha^3-3\alpha)\cosh\alpha + 3\sinh\alpha]}\Bigg([180+(90y^2-30)\alpha^2]e^{-\alpha} + 360\alpha\cosh(\alpha y) - 15\alpha^5\left(y^4-2y^2+\frac{7}{15}\right)\cosh\alpha - 90e^{\alpha}\left\{\left[2+\alpha^2\left(y^2-\frac{1}{3}\right)\right]\right\}\Bigg), \tag{39}$$

$$M(y) = -\frac{y^2}{2} - \frac{(\beta_1-\beta_2)y}{\beta_1+\beta_2} + \frac{1}{6}. \tag{40}$$

We extract the second-order perturbation, which corresponds to $O(\epsilon^2)$, using Eqs. (13), (16), and (20)–(22):

$$\frac{\partial C^{(0)}}{\partial t_2} + \frac{\partial C^{(1)}}{\partial t_1} + \frac{\partial C^{(2)}}{\partial t_0} + \mathrm{Pe}\, u_x\frac{\partial C^{(1)}}{\partial x} = \frac{\partial^2 C^{(0)}}{\partial x^2} + \frac{\partial^2 C^{(2)}}{\partial y^2} - KC^{(0)}, \quad -1 < y < 1, \tag{41}$$

and

$$\left(\frac{\partial C^{(2)}}{\partial y} - \beta_2 C^{(1)}\right)\Big|_{y=-1} = 0, \quad \left(\frac{\partial C^{(2)}}{\partial y} + \beta_1 C^{(1)}\right)\Big|_{y=1} = 0. \tag{42}$$

Since the time variable $t_0$ is significantly larger than both $t_1$ and $t_2$, the term $\frac{\partial C^{(2)}}{\partial t_0}$ is negligible compared to $\frac{\partial C^{(1)}}{\partial t_1}$ and $\frac{\partial C^{(0)}}{\partial t_2}$. Therefore, $\frac{\partial C^{(2)}}{\partial t_0}$ is neglected from Eq. (41):

$$\frac{\partial C^{(0)}}{\partial t_2} + \frac{\partial C^{(1)}}{\partial t_1} + \mathrm{Pe}\, u_x\frac{\partial C^{(1)}}{\partial x} = \frac{\partial^2 C^{(0)}}{\partial x^2} + \frac{\partial^2 C^{(2)}}{\partial y^2} - KC^{(0)}. \tag{43}$$

Computing the sectional average of Eq. (43) concerning the spatial variable $y$ and considering the boundary conditions in Eqs. (42), we have

$$\frac{\partial C^{(0)}}{\partial t_2} + \frac{\partial\langle C^{(1)}\rangle}{\partial t_1} + \mathrm{Pe}\left\langle u_x\frac{\partial C^{(1)}}{\partial x}\right\rangle = \frac{\partial^2 C^{(0)}}{\partial x^2} - \frac{1}{2}(\beta_1 C^{(1)}(1) + \beta_2 C^{(1)}(-1)) - KC^{(0)}. \tag{44}$$

Using Eqs. (32), (35), and (44) the terms of Eq. (44) are found as

$$\frac{\partial\langle C^{(1)}\rangle}{\partial t_1} = 0, \quad \left\langle u_x\frac{\partial C^{(1)}}{\partial x}\right\rangle = \mathrm{Pe}\,\langle u_x N\rangle\frac{\partial^2 C^{(0)}}{\partial x^2} + \frac{1}{2}(\beta_1+\beta_2)\langle u_x M\rangle\frac{\partial C^{(0)}}{\partial x}. \tag{45}$$

Substituting these terms in Eq. (44), we get

$$\frac{\partial C^{(0)}}{\partial t_2} + \mathrm{Pe}\left[\frac{1}{2}(\beta_1+\beta_2)\langle u_x M\rangle + \frac{\beta_1}{2}N(1) + \frac{\beta_2}{2}N(-1)\right]\frac{\partial C^{(0)}}{\partial x} = (1-Pe^2\langle u_x N\rangle)\frac{\partial^2 C^{(0)}}{\partial x^2} - \frac{1}{4}(\beta_1+\beta_2)[\beta_2 M(-1)+\beta_1 M(1)]C^{(0)} - KC^{(0)}. \tag{46}$$

Further, by rewriting Eq. (46) in original time variables, as

$$\frac{\partial C^{(0)}}{\partial t} + \epsilon\,\mathrm{Pe}\,\chi\frac{\partial C^{(0)}}{\partial x} = \epsilon^2 D_T\frac{\partial^2 C^{(0)}}{\partial x^2} - \zeta C^{(0)}, \tag{47}$$

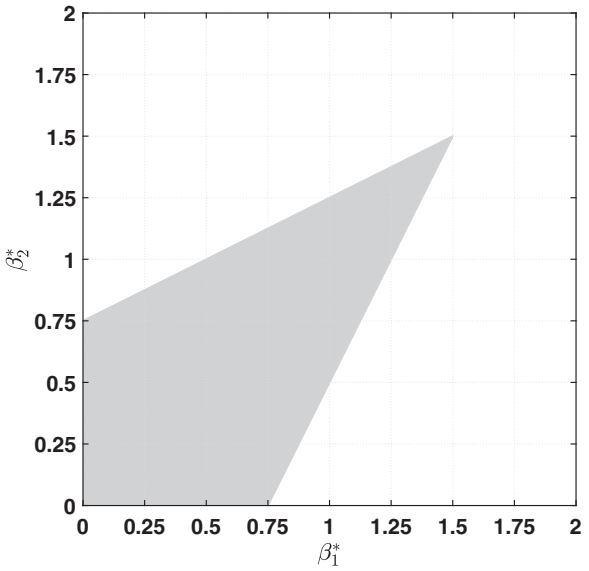


FIG. 2. Shaded region delineating the valid ranges for $\beta_1^*$ and $\beta_2^*$ where $\zeta$ is valid, for any $K^* \geqslant 0$.

where $\chi$, $D_T$, and $\zeta$ are the advection, dispersion, and reaction coefficients, respectively, the expressions are as follows:

$$\chi = \langle u_x \rangle + \tfrac{1}{2}[(\beta_1^* + \beta_2^*)\langle u_x M \rangle + \beta_1^* N(1) + \beta_2^* N(-1)], \tag{48}$$

$$D_T = 1 - \mathrm{Pe}^2 \langle u_x N \rangle, \tag{49}$$

and

$$\zeta = \tfrac{1}{2}(\beta_1^* + \beta_2^*) + \tfrac{1}{4}(\beta_1^* + \beta_2^*)[\beta_2^* M(-1) + \beta_1^* M(1)] + K^*. \tag{50}$$

Here, $\beta_1^* (= \frac{\beta_1' h}{D} = \epsilon \beta_1)$, $\beta_2^* (= \frac{\beta_2' h}{D} = \epsilon \beta_2)$ and $K^* (= \frac{k h^2}{D} = \epsilon^2 K)$ are the new dimensionless variables.

For a significant nonzero exponential decrease in solute concentration caused by reactions, the term $\zeta(\beta_1^*, \beta_2^*, K^*) = \frac{1}{2}(\beta_1^* + \beta_2^*) - \frac{1}{3}(\beta_1^{*2} + \beta_2^{*2} - \beta_1^* \beta_2^*) + K^*$ must satisfy the conditions $\zeta(\beta_1^*, \beta_2^*, K^*) \geqslant \zeta(\beta_1^* - \varepsilon_1, \beta_2^*, K^*) > 0$ and $\zeta(\beta_1^*, \beta_2^*, K^*) \geqslant \zeta(\beta_1^*, \beta_2^* - \varepsilon_2, K^*) > 0$, where $0 \leqslant \varepsilon_1 \leqslant \beta_1^*$, $0 \leqslant \varepsilon_2 \leqslant \beta_2^*$ and $K^* \geqslant 0$ (but $\beta_1^*$, $\beta_2^*$, and $K^*$ are not simultaneously zero). These conditions are crucial for satisfying the physical principle that increasing the reaction terms reduces the concentration within the system. Conversely, the reduction in one or more reaction terms will result in increasing the concentration. Thus the valid region for $\zeta(\beta_1^*, \beta_2^*, K^*)$ has been drawn (see Fig. 2) to ensure the consistency with the governing physics. The shaded area in Fig. 2 represents the ranges for $\beta_1^*$ and $\beta_2^*$ (for any fixed $K^*$) for which $\zeta$ is valid, and thus the analytical solution (including the case $\zeta = 0$, when $\beta_1^* = \beta_2^* = K^* = 0$) [56]. Using the initial and boundary conditions given in Eqs. (6)–(9), the solution of Eq. (47) in new variable $\tau = t$ and $\xi = \frac{x'}{h} - \mathrm{Pe}\chi t$ can be expressed as

$$C^{(0)} = \frac{1}{\sqrt{4\pi D_T \tau}} \exp\left(-\frac{\xi^2}{4 D_T \tau} - \zeta \tau\right). \tag{51}$$

Here, the newly introduced coordinate system $\{\xi, \tau\}$ makes it possible to observe the mass transport phenomena from a reference frame moving at a speed of Pe $\chi$. The second-order concentration

can be obtained by subtracting Eq. (44) from Eq. (41) as follows:

$$\frac{\partial C^{(1)}}{\partial t_1} + \mathrm{Pe}\left[u_x \frac{\partial C^{(1)}}{\partial x} - \left\langle u_x \frac{\partial C^{(1)}}{\partial x}\right\rangle\right] = \frac{\partial^2 C^{(2)}}{\partial y^2} + \frac{1}{2}[\beta_1 C^{(1)}(1) + \beta_2 C^{(1)}(-1)]. \tag{52}$$

On taking the derivative of the concentration $C^{(1)}$ with respect to $t_1$ and substituting Eq. (30), we get

$$\begin{aligned}\frac{\partial C^{(1)}}{\partial t_1} =& -\mathrm{Pe}^2\langle u_x\rangle N(y)\frac{\partial^2 C^{(0)}}{\partial x^2} - \frac{1}{2}\mathrm{Pe}\,(\beta_1+\beta_2)[N(y)+\langle u_x\rangle M(y)]\frac{\partial C^{(0)}}{\partial x}\\ &- \frac{1}{4}(\beta_1+\beta_2)^2 M(y) C^{(0)}.\end{aligned} \tag{53}$$

Using Eqs. (32), (45), and (53) in Eq. (52), we get

$$\begin{aligned}&\mathrm{Pe}^2[u_x N - \langle u_x\rangle N - \langle u_x N\rangle]\frac{\partial^2 C^{(0)}}{\partial x^2} + \frac{1}{2}\mathrm{Pe}\,(\beta_1+\beta_2)\\ &\times\left[u_x M - N - \langle u_x\rangle M - \langle u_x M\rangle - \frac{\beta_1 N(1)+\beta_2 N(-1)}{\beta_1+\beta_2}\right]\frac{\partial C^{(0)}}{\partial x}\\ &+\frac{1}{4}(\beta_1+\beta_2)^2\left[-M - \frac{\beta_1}{\beta_1+\beta_2}M(1) - \frac{\beta_2}{\beta_1+\beta_2}M(-1)\right]C^{(0)} = \frac{\partial^2 C^{(2)}}{\partial y^2}.\end{aligned} \tag{54}$$

By applying a procedure analogous to that used for first order, we can derive the second-order terms in the following form:

$$C^{(2)} = \mathrm{Pe}^2 X(y)\frac{\partial^2 C^{(0)}}{\partial x^2} + \frac{1}{2}(\beta_1+\beta_2)\mathrm{Pe}\,Y(y)\frac{\partial C^{(0)}}{\partial x} + \frac{1}{4}(\beta_1+\beta_2)^2 Z(y) C^{(0)}, \tag{55}$$

the second-order transverse functions ($X$, $Y$, and $Z$) of which are delineated in the Supplemental Material [57].

For the third-order perturbation $O(\epsilon^3)$, using Eqs. (13), (16), and (20)–(22), we get

$$\frac{\partial C^{(1)}}{\partial t_2} + \frac{\partial C^{(2)}}{\partial t_1} + \frac{\partial C^{(3)}}{\partial t_0} + \mathrm{Pe}\,u_x\frac{\partial C^{(2)}}{\partial x} = \frac{\partial^2 C^{(1)}}{\partial x^2} + \frac{\partial^2 C^{(3)}}{\partial y^2} - K C^{(1)}, \quad -1 < y < 1, \tag{56}$$

and

$$\left(\frac{\partial C^{(3)}}{\partial y} - \beta_2 C^{(2)}\right)\Big|_{y=-1} = 0, \quad \left(\frac{\partial C^{(3)}}{\partial y} + \beta_1 C^{(2)}\right)\Big|_{y=1} = 0. \tag{57}$$

By averaging Eqs. (56) and (57) over the spatial variable $y$ and combining the terms associated with $\frac{\partial^2 C^{(0)}}{\partial x^2}$, we get the dispersion coefficient ($D_{T\beta}$) involving wall reaction parameters as

$$D_{T\beta} = \mathrm{Pe}^2\frac{\beta_1^* + \beta_2^*}{2}\left[-\langle u_x Y\rangle - \frac{\beta_1^* X(1) + \beta_2^* X(-1)}{\beta_1^* + \beta_2^*}\right]. \tag{58}$$

Following a procedure similar to that utilized in the first order, we can express the developed terms in the third order as

$$\begin{aligned}C^{(3)} =& \mathrm{Pe}^3 P(y)\frac{\partial^3 C^{(0)}}{\partial x^3} + \frac{1}{2}\mathrm{Pe}^2(\beta_1+\beta_2)Q(y)\frac{\partial^2 C^{(0)}}{\partial x^2}\\ &+\frac{1}{4}\mathrm{Pe}(\beta_1+\beta_2)^2 R(y)\frac{\partial C^{(0)}}{\partial x} + \frac{1}{8}(\beta_1+\beta_2)^3 S(y) C^{(0)},\end{aligned} \tag{59}$$

the transverse functions of the third orders ($P$, $Q$, $R$, and $S$) of which can be found in the Supplemental Material [57].

## IV. NUMERICAL SIMULATION

In an earlier section, following the asymptotic expansion given in Eq. (20), we obtained the analytical solution of the two-dimensional concentration distribution up to third order, and it can be written as follows:

$$\begin{aligned} C &= C^{(0)} + \epsilon C^{(1)} + \epsilon^2 C^{(2)} + \epsilon^3 C^{(3)} \\ &= \left(1 + \frac{1}{2}(\beta_1^* + \beta_2^*)M(y) + \frac{1}{4}(\beta_1^* + \beta_2^*)^2 Z(y) + \frac{1}{8}(\beta_1^* + \beta_2^*)^3 S(y)\right) C^{(0)} \\ &\quad + \mathrm{Pe}\left(N(y) + \frac{1}{2}(\beta_1^* + \beta_2^*)Y(y) + \frac{1}{4}(\beta_1^* + \beta_2^*)^2 R(y)\right)\frac{\partial C^{(0)}}{\partial \xi} \\ &\quad + \mathrm{Pe}^2\left(X(y) + \frac{1}{2}(\beta_1^* + \beta_2^*)Q(y)\right)\frac{\partial^2 C^{(0)}}{\partial \xi^2} + \mathrm{Pe}^3 P(y)\frac{\partial^3 C^{(0)}}{\partial \xi^3}. \end{aligned} \tag{60}$$

To further explore the results from the above solution, we will first develop a numerical model for the advection-diffusion equation [see Eq. (13)], along with its corresponding initial and boundary conditions in Eqs. (14)–(17), which can be rewritten using the dimensional space and time variables $\{\xi, \tau\}$ as

$$\frac{\partial C}{\partial \tau} + \mathrm{Pe}(u_x - \chi)\frac{\partial C}{\partial \xi} = \frac{\partial^2 C}{\partial \xi^2} + \frac{\partial^2 C}{\partial y^2} - K^* C, \quad -1 \leqslant y \leqslant 1, \tag{61}$$

$$C(\xi, y, \tau)|_{\tau=0} = \delta(\xi), \tag{62}$$

$$\left.\frac{\partial C}{\partial y}\right|_{y=1} = -\beta_1^* C(\xi, 1, \tau), \tag{63}$$

$$\left.\frac{\partial C}{\partial y}\right|_{y=-1} = \beta_2^* C(\xi, -1, \tau), \tag{64}$$

$$C(\xi, y, \tau)|_{\xi \to \pm\infty} = 0. \tag{65}$$

To validate the accuracy of the analytical solution, a numerical simulation [56] for the given system of Eqs. (61)–(65) has been conducted. The computational domain employed for discretization is a rectangular domain with dimensions of 20-in. length and 2-in. width. This domain extends from $-10$ to 10 along the $x$ direction and from $-1$ to 1 in the $y$ direction. The unsteady term and the advection term from Eq. (61) are discretized using the first-order forward difference scheme and the first-order upwind scheme, respectively. We discretized the diffusion terms corresponding to the second derivatives of the spatial variables using the second-order central difference scheme. The discretized form of the governing equation Eq. (61), excluding the truncation error terms, is as follows:

$$\begin{aligned} &\frac{C_{i,j}^{n+1} - C_{i,j}^n}{\Delta\tau} + Pe\left\{\max(u_x - \chi, 0)\frac{C_{i,j}^n - C_{i-1,j}^n}{\Delta\xi} - \max(\chi - u_x, 0)\frac{C_{i+1,j}^n - C_{i,j}^n}{\Delta\xi}\right\} \\ &= \frac{C_{i+1,j}^n - 2C_{i,j}^n + C_{i-1,j}^n}{(\Delta\xi)^2} + \frac{C_{i,j+1}^n - 2C_{i,j}^n + C_{i,j-1}^n}{(\Delta y)^2} - K^* C_{i,j}^n, \end{aligned} \tag{66}$$

where $i = 1, 2, \ldots, I-1$ and $j = 1, 2, \ldots, J-1$, where $I$ and $J$ represent the maximum number of subintervals along the $\xi$ and $y$ directions, respectively.

The boundary conditions in Eqs. (63) and (64) are discretized using three-point backward and forward schemes, leading to the following discretized forms:

$$\frac{3C_{i,J}^{n+1} - 4C_{i,J-1}^n + C_{i,J-2}^n}{2\Delta y} = -\beta_1^* C_{i,J}^{n+1}, \quad i = 0, 1, \ldots, I, \tag{67}$$

and

$$\frac{-C_{i,2}^{n}+4C_{i,1}^{n}-3C_{i,0}^{n+1}}{2\Delta y}=\beta_2^* C_{i,0}^{n+1},\quad i=0,1,\ldots,I. \tag{68}$$

The discretized expression of Eq. (65) is given by

$$C_{0,j}^{n+1}=0,\quad \text{and } C_{I,j}^{n+1}=0,\quad j=0,1,\ldots,J. \tag{69}$$

The discretized expression of the initial condition Eq. (62) is given by

$$C_{i,j}^{n}=\begin{cases}0 & 0\leqslant i\leqslant I,\ \ 0\leqslant j\leqslant J,\ \ i\neq I/2,\\ 50 & i=I/2,\ \ 0\leqslant j\leqslant J.\end{cases} \tag{70}$$

Here, $\Delta\tau=\frac{0.4}{(1/\Delta\xi)^2+(1/\Delta y)^2}$, where $\Delta\xi=\Delta\xi_i=\xi_{i+1}-\xi_i=1/50$ and $\Delta y=\Delta y_j=y_{j+1}-y_j=1/50$. We consider the Dirac delta function $\delta(\xi)$ as follows: $\delta(\xi)=0$ for $\xi\neq 0$, and $\delta(0)=50$, following the definition and standard property of the Dirac delta function, which states that $\int_{-\infty}^{\infty}\delta(\xi)d\xi\approx\int_{-10}^{10}\delta(\xi)d\xi\approx\sum_{i=0}^{I}\delta(\xi_i)\Delta\xi_i=1$.

## V. RESULT AND DISCUSSION

This section embarks on a comprehensive exploration of the complex phenomenon of longitudinal dispersion that occurs within the horizontal channel flow of a viscous couple stress fluid. This paper meticulously examines the influence of couple stress on crucial aspects of the flow dynamics, including the velocity profile following Taylor's dispersivity, mean concentration, and transverse concentration. Moreover, this paper extends its analysis to incorporate various parameters, including $\beta_1^*$, $\beta_2^*$, $K^*$, and $\alpha$, providing an insight into how these parameters impact the distributions of mean and transverse concentrations. This paper sheds light on the intricate relationship between the significant variations in these parameters and their corresponding impact on the variations in the concentration distributions. Furthermore, it is noteworthy that the parameters $\alpha$ and Pe influence Taylor's dispersivity, which characterizes solute dispersion, mixing, and spreading. Particularly in physiological systems (blood vessels or microfluidic channels), the dispersion coefficient has a significant impact because of the couple stress parameter $\alpha$, which characterizes the interaction between the fluid and the channel geometry. This parameter $\alpha$ generally depends on the size of the fluid element or the suspended particles (nanoparticles or biological components) present in the fluid. Hence, this paper delves into the manifestations of these factors within the distributions of mean and transverse concentrations to elucidate their significance for Taylor's dispersivity. The present paper relies on several assumptions to elucidate the effect of couple stress and chemical reactions. Moreover, these results have certain limitations, especially when dealing with microscale channels for smaller values of $\alpha$ (i.e., $\alpha\ll 1$). When $\alpha$ is very small, say $\alpha=0.001$, 0.01, or 0.05, chaotic conditions arise due to the fluid's internal structure, leading to a complex interplay between the effects of couple stress and viscosity, which makes the results less reliable in this range. The role of parameters $\alpha$, $\beta_1^*$, $\beta_2^*$, and $K^*$ is more crucial in observing the intricate behavior of the solutes within this system. Additionally, we assumed $Pe=O(1)$ indicating that advection and diffusion are comparable, to investigate the mean and transverse concentration distributions. The ranges of various parameters used in this paper are listed in Table I.

### A. Velocity profile

Figure 3 depicts the influence of the couple stress parameter $\alpha$ on flow velocity, illustrating the velocity variation ($u_x$) as a function of the dimensionless width ($y$) for various values of $\alpha$. Stokes [13] determined the velocity taken into consideration in this paper. Since the velocity distribution considered in this paper depends on $\alpha$ [see Eq. (18)], the influence of couple stress becomes apparent in altering the velocity profile within a horizontal channel flow with viscous fluid. Figure 3 visually portrays that the velocity takes its maximum values at the center of the channel since the

TABLE I. Ranges of various dimensionless parameters utilized in the present paper.

| Parameters | Minimum | Maximum |
|---|---|---|
| $\xi$ | $-\infty$ | $\infty$ |
| $y$ | $-1$ | 1 |
| $\alpha$ | 1 | 100 |
| $\beta_1^*/\beta_2^*$ | 0 | 1.5 |
| $K^*$ | 0 | 4 |
| $\tau$ | 0.25 | 100 |

velocity profile is parabolic and zero at the channel plates due to the no-slip condition. Furthermore, increasing $\alpha$ leads to a subtle increase in velocity between the channel plates and the center of the channel due to the weaker effect of couple stress that allows the fluid to experience rotational deformation. However, as the fluid particles move toward the center, the viscosity is dominant, which counteracts the velocity rise, leading to a subtle decrease for increasing values of $\alpha$. Similarly, in the case of decreasing $\alpha$, the strong influence of a couple stress effect relative to viscosity will resist the rotational deformation near the plates. However, at the center of the channel, the velocity distribution experiences an increase due to the minimal influence of viscosity. In other words, as $\alpha$ decreases, the dominance of couple stress over viscosity increases, resulting in higher velocities at the center of the channel compared to higher values of $\alpha$. This behavior is particularly noticeable in liquids with large molecules, such as polymer chains, which may be significantly longer than the diameter of a water molecule, allowing couple stress to appear in noticeable magnitudes [53]. This reflects the strong impact of molecular dimensions on the velocity profile. Moreover, higher $\alpha$ values, on the other hand, may cause a reduction in velocity distribution at the center because of the dominant viscosity [58]. Physically, this implies that for very small molecular additives or fluids with smaller chain lengths, the couple stress effects are negligible, resulting in a flow similar to that of a purely viscous fluid. Hence, for $\alpha \leqslant 20$, the influence of couple stress on the velocity profile is both significant and consistent, strongly affecting the flow dynamics. However, for $\alpha > 20$ the influence becomes more subtle, and the behavior of the velocity profile approaches that observed at $\alpha = 20$ even for higher values. Notably, it is evident from Fig. 3 for $\alpha \gg 20$ that there is a subtle decrease in velocity due to the dominant effect of viscosity compared with couple stress at the

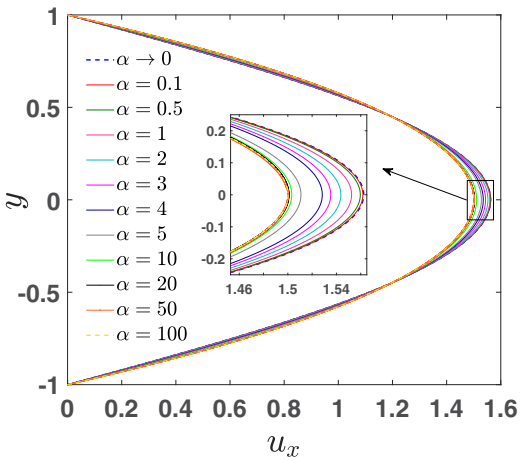


FIG. 3. Variation in velocity profiles with varying couple stress parameter $\alpha$.

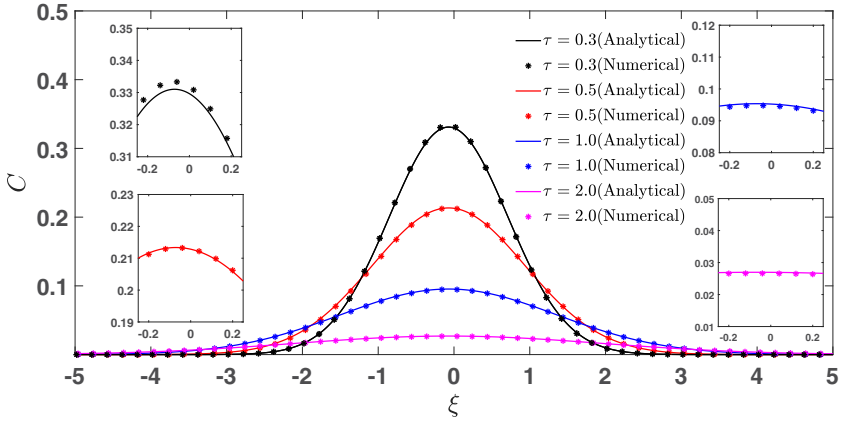


FIG. 4. Comparison between analytical and numerical results of two-dimensional concentration distribution for different times with $\alpha = 1$, $\beta_1^* = \beta_2^* = 0.5$, and $K^* = 0.5$ at $y = 1$.

center of the channel. This suggests that for very large $\alpha$, the couple stress effects are present but increasingly negligible, with the flow behaving similarly to that of the classical plane Poiseuille case. Thus, varying the couple stress parameter $\alpha$ illustrates the transition between complex behaviors influenced by couple stresses and the classical plane Poiseuille flow [23].

### B. Numerical validation

To verify the accuracy of the present analytical result derived using a multiscale homogenization technique, a comparison is made with numerical solutions of the governing equation with the help of associated initial and boundary conditions. A comparative analysis of analytical and numerical results of the present paper is shown in Figs. 4–6 for the two-dimensional concentration distribution at the channel's plate ($y = 1$) when the couple stress parameter $\alpha = 1$. The figures showcase a good alignment between our analytical and numerical results. However, from Fig. 4, we observe during the initial time ($\tau < 1$) that there are some discrepancies in aligning the analytical results with their numerical counterparts. The minor discrepancies found in the paper imply that the results may not be entirely dependable in the initial period. Despite these early inconsistencies, for $\tau > 1$, the long-term asymptotic dispersion model provides more accuracy and precisely captures the temporal evolution of the transverse concentration distribution.

Figure 5(a) compares the numerical and analytical results for different Pe values. The analytical and numerical results agree well for smaller Pe values, particularly for $\mathrm{Pe} = 0.5$ and 1. However, a significant discrepancy appears at $\mathrm{Pe} \geqslant 10$. Therefore, when $\mathrm{Pe} = O(1)$, the analytical solution fits well with the numerical simulation. Figure 5(b) validates the analytical results against numerical data for varying bulk chemical reaction parameters. The results show a strong agreement, particularly as $K^*$ increases.

Figure 6 deliberately compares the analytical and numerical results for various values of wall chemical reaction parameters. The analytical results closely match the numerical ones when $\beta_1^* = \beta_2^* = \beta^* \leqslant 1$. However, as $\beta^*$ increases, significant differences arise between the analytical and numerical results. Moreover, when the wall chemical reaction is introduced on either of the plates, the analytical and numerical results match well for lower values of the wall chemical reaction parameters, such as $\beta_1^* = 0$ and $\beta_2^* \leqslant 0.75$ or $\beta_1^* \leqslant 0.75$ and $\beta_2^* = 0$. The notable disparity between the analytical and numerical results arises when the wall chemical reaction parameters exceed 1. Although there is some variation in the analytical and numerical results when the wall chemical reaction parameter exceeds 1, the analytical solution remains valid within the range where $\beta^* \leqslant 1.5$ as illustrated in Fig. 2.

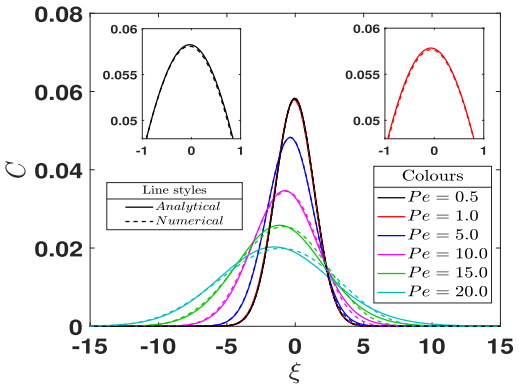


(a) $K^* = 1$

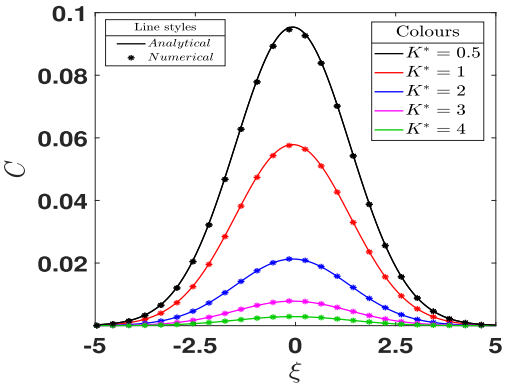


(b)

FIG. 5. Comparison between analytical and numerical results of two-dimensional concentration distribution with $\alpha = 1$, $\beta_1^* = \beta_2^* = 0.5$, and $y = 1$ at $\tau = 1$ for different (a) Pe and (b) $K^*$.

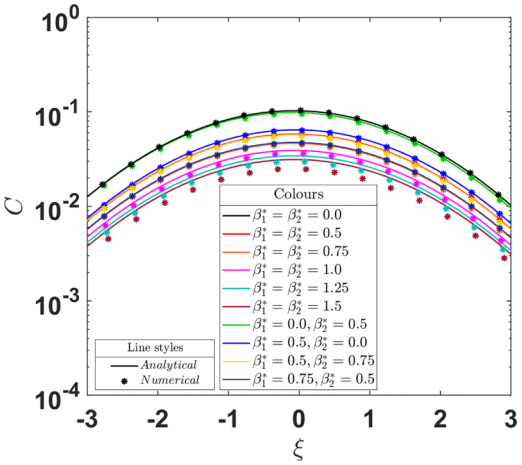


FIG. 6. Comparison between analytical and numerical results of two-dimensional concentration distribution for different wall chemical reaction parameters ($\beta_1^*$ and $\beta_2^*$), where $y = 1$, $\alpha = 1$, and $K^* = 1$ at $\tau = 1$.

TABLE II. Comparison of the magnitude of dispersion coefficient $D_{Tc}$ and the previous [23] for distinct couple stress parameter $\alpha$.

| $\alpha$ | 1 | 10 | 20 | 50 | $\infty$ |
|---|---|---|---|---|---|
| Present paper | 0.0222 | 0.0197 | 0.0193 | 0.0191 | 0.0190 |
| Rudraiah *et al.* [23] | 0.0220 | 0.0190 | 0.0190 | 0.0190 | 0.0190 |

### C. Dispersion coefficient

The equation representing the effective overall dispersion coefficient can be reformulated from Eqs. (49) and (58) as

$$D_T = 1 + \mathrm{Pe}^2 D_T^*, \tag{71}$$

where $D_T^* (= D_{Tc} + D_{T\beta})$ denotes the apparent dispersion coefficients, where $D_{Tc}$ $(= -\langle u_x N\rangle)$ encapsulates the combined effects of lateral diffusion and advection, and $D_{T\beta}$ represents the additional effect due to wall chemical reactions. The contribution of longitudinal diffusion is isolated within the first term on the right side of Eq. (71), specifically the constant term, which equals 1. We can accentuate the significance of lateral diffusion and advection by omitting this constant term (i.e., 1). From Eq. (71), the explicit form of the dispersion coefficients can be expressed as

$$\begin{aligned} D_{Tc} = {} & \frac{1}{840\{-9 + (\alpha^6 - 6\alpha^4 + 9\alpha^2 + 9)\cosh^2\alpha + 6\alpha(\alpha^2 - 3)\sinh\alpha\cosh\alpha\}\alpha^2} \\ & \times \{(4\alpha^8 + 84\alpha^5 - 1260\alpha^3 - 3150\alpha^2 - 945\alpha + 3780)e^{-2\alpha} \\ & + (4\alpha^8 - 84\alpha^5 + 1260\alpha^3 - 3150\alpha^2 + 945\alpha + 3780)e^{2\alpha} + 8\alpha^8 - 12\,600\alpha^2 - 7560\}, \end{aligned} \tag{72}$$

$$\begin{aligned} D_{T\beta} = {} & -\frac{(\beta_1^* + \beta_2^*)[-9 + (\alpha^6 - 6\alpha^4 + 9\alpha^2 + 9)\cosh^2\alpha - 6(\alpha^3 - 3\alpha)\sinh\alpha\cosh\alpha]}{1575\{9 + (\alpha^6 - 6\alpha^4 + 9\alpha^2 - 9)\cosh^2\alpha\}^2\alpha^4} \\ & \times \left\{\left(\alpha^{10} + 45\alpha^7 + \frac{315}{2}\alpha^6 - \frac{945}{2}\alpha^5 - 6615\alpha^4 - \frac{231\,525}{8}\alpha^3 - \frac{978\,075}{16}\alpha^2 - \frac{1\,318\,275}{32}\alpha \right.\right. \\ & \left. + \frac{70\,875}{2}\right)e^{-2\alpha} + \left(\alpha^{10} - 45\alpha^7 + \frac{315}{2}\alpha^6 + \frac{945}{2}\alpha^5 - 6615\alpha^4 + \frac{231\,525}{8}\alpha^3 - \frac{978\,075}{16}\alpha^2 \\ & \left. + \frac{1\,318\,275}{32}\alpha + \frac{70\,875}{2}\right)e^{2\alpha} + 2\alpha^{10} + 315\alpha^6 - 15\,120\alpha^4 - 184\,275\alpha^2 - 70\,875\right\}. \end{aligned} \tag{73}$$

When $\alpha$ approaches infinity, the dispersion of the solute becomes independent of couple stress. The limiting value of $D_T$ at $\alpha \to \infty$ is determined as

$$D_T = 1 + \mathrm{Pe}^2\left\{\frac{2}{105} - \frac{4}{1575}(\beta_1^* + \beta_2^*)\right\}. \tag{74}$$

In the absence of wall chemical reaction (i.e., when $\beta_1^* = \beta_2^* = 0$ or $D_{T\beta} = 0$) Eq. (74) becomes

$$D_T|_{\alpha\to\infty} = 1 + \frac{2}{105}\,\mathrm{Pe}^2, \tag{75}$$

where the apparent dispersion coefficient $D_{Tc} = \frac{2}{105} = 0.0190$ (approximately) [23,40,52].

Table II compares the $D_{Tc}$ values obtained in the present paper with a previous study for distinct values of the parameter $\alpha$ to validate the existing results obtained in this paper. From the comparison,

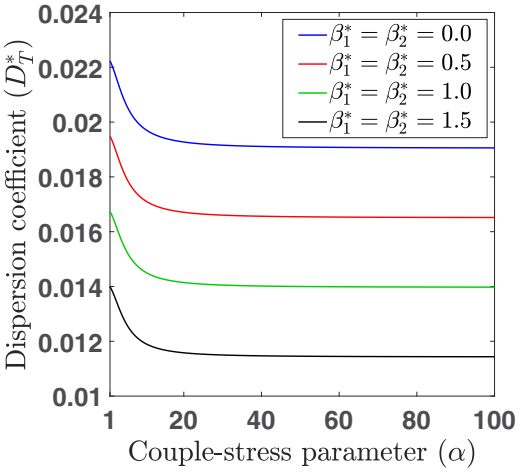


FIG. 7. Variation of $D_T^*$ with $\alpha$ and $\beta^*$, where $\beta_1^* = \beta_2^* = \beta^*$.

it is clear that there is good agreement between the values of the dispersion coefficient, which suggests the validity and reliability of the current analytical solution.

In the present paper, solute dispersion is contingent upon the combined effect of advection and diffusion, the influence of the couple stress, and the additional impact of wall chemical reaction. Typically, the couple stress refers to the internal rotational forces within the fluid that influence the rotational deformation of the fluid element at a microscale. Couple stress generally arises due to the nonsymmetric distribution of forces or stresses within a fluid element. Figure 7 provides insights into how the parameter $\alpha$ influences the dispersion coefficient. It is noteworthy that there is an abnormal behavior in dispersion for $\alpha \ll 1$ since there is an intricate interplay between the influence of couple stress and viscosity. Less viscosity than couple stress induces the solute to disperse more efficiently, but on the other hand, the high couple stress increases resistance in the solute molecule's rotational deformation. Also, as $\alpha \to 0$, the internal structure of the fluid becomes more significant, leading to the strong interaction between the fluid elements that potentially hinders the movement and influences the dispersion. For very low $\alpha$, these interactions become intricate in understanding the behavior of the system and the couple stress effect, which might result in inaccuracy in representing them. These inconsistent natures result in unexpected distributions and interactions in solute dispersion for $\alpha \to 0$. To elucidate the intricate relation of the parameter $\alpha$ and $D_T^*$ concerning the additional effect of $\beta_1^*$ and $\beta_2^*$, Fig. 7 has been drawn for the range $1 \leqslant \alpha \leqslant 100$ against $D_T^*$ for distinct values of wall chemical reaction parameters. For $\alpha < 20$, the strong influence of couple stress will contribute intricate microscale internal force, which enhances the mixing and dispersion of the solute particles. Also, the viscosity is minimal compared to the couple stress effect, and makes it easier for the solute to disperse, increasing the dispersion coefficient. As $\alpha$ increases, the couple stress decreases and the viscous effect becomes more efficient than couple stress, which makes it more difficult for the solute to disperse effectively. For $\alpha < 20$, the combined effect of diffusion and couple stress will become prominent. They dominate over advection, which provokes the solute to be dispersed more rapidly by the fluid. However, for $\alpha \gg 20$, the influence of couple stress is less than viscosity, indicating less resistance in the solute molecules' rotational deformation that induces less mixing and dispersion. As a result, the dispersion coefficient eventually has a minimal decrease for $\alpha \gg 20$. In simpler terms, an increase in $D_T^*$ corresponds to an increase in the velocity parameter $u_x$, while a decrease in $D_T^*$ is associated with a reduction in $u_x$. Additionally, the impact of the wall chemical reaction parameters is depicted in Fig. 7. Increasing the wall chemical reaction parameters leads to a decrease in solute dispersion. This is because stronger wall reactions effectively remove (i.e., absorb) the solute molecules from the system near the

TABLE III. Dispersion coefficient magnitude $D_{Tc}$ corresponding to distinct values of couple stress parameter $\alpha$.

| $\alpha$ | 1 | 5 | 10 | 15 | 20 | 25 | 30 | 35 | 40 | 45 | 50 | 100 | 200 | $\infty$ |
|---|---|---|---|---|---|---|---|---|---|---|---|---|---|---|
| $D_{Tc}$ | 0.0222 | 0.0207 | 0.0197 | 0.0194 | 0.0193 | 0.0192 | 0.0192 | 0.0191 | 0.0191 | 0.0191 | 0.0191 | 0.0191 | 0.0191 | 0.0190 |

wall, thereby limiting the overall dispersion of the solute. It is noteworthy from the figure that when $\alpha \ll 20$, couple stress has a more significant impact, whereas, for $\alpha \gg 20$, the influence of couple stress on solute dispersion becomes negligible. This characteristic exactly matches the result obtained by Soundalgekar [20]. Furthermore, the explicit values given in Table III ensure a subtle reduction in the dispersion coefficient as the value of the couple stress parameter $\alpha$ increases, as illustrated in Fig. 7.

### D. Mean concentration

From Eqs. (20) and (51), the mean concentration can be determined as

$$\langle C\rangle = C^{(0)} = \frac{1}{\sqrt{4\pi D_T \tau}} \exp\left[ -\frac{\xi^2}{4D_T\tau} - \left\{ \frac{1}{2}(\beta_1^* + \beta_2^*) - \frac{1}{3}\left(\beta_1^{*2} + \beta_2^{*2} - \beta_1^*\beta_2^*\right) + K^* \right\}\tau \right]. \quad (76)$$

To induce the impact of lateral diffusion in mean concentration, we express the dispersion coefficient as $D_T^*\mathrm{Pe}^2$. Consequently, we can rewrite the aforementioned Eq. (76) in the new coordinate system $\{\xi/\mathrm{Pe}, \langle C\rangle \mathrm{Pe}\}$ as

$$\langle C\rangle\ \mathrm{Pe} = \frac{1}{\sqrt{4\pi D_T^* \tau}} \exp\left[ -\frac{1}{4D_T^*\tau}\left(\frac{\xi}{\mathrm{Pe}}\right)^2 - \left\{ \frac{1}{2}(\beta_1^* + \beta_2^*) - \frac{1}{3}\left(\beta_1^{*2} + \beta_2^{*2} - \beta_1^*\beta_2^*\right) + K^* \right\}\tau \right]. \quad (77)$$

The mean concentration distribution of a solute in the channel flow is affected by various parameters, and those are illustrated in Fig. 8. Figure 8(a) showcases the influence of the couple stress parameter $\alpha$ in mean concentration distribution. When $\alpha < 20$, the influence of couple stress is high when compared with viscosity for decreasing $\alpha$, which increases the dispersion of the solute; as a result, the mean concentration distribution decreases. Furthermore, when $\alpha \geqslant 20$ this increases the mean concentration due to minimal solute dispersion. Because the fluid is less likely to flow and transport the solute molecules when the couple stress effect is less, moreover, due to low-velocity distribution, the mean concentration distribution is slightly higher for $\alpha = 50$ and 100 compared to smaller values of $\alpha$, and it decreases for $\alpha < 20$ with an amplification in the longitudinal dispersion. Figure 8(b) demonstrates how variations in the wall chemical reaction parameters affect the mean concentration distribution. The wall chemical reaction parameters represent the rate at which the channel's boundaries absorb the solute molecules at the channel's plate. Increased values of wall chemical reaction parameters cause the plates to absorb more solute molecules, thereby decreasing the mean concentration distribution. The absence of wall chemical reactions at the channel's plates increases the mean concentration distribution since there will be no reactions to reduce the mean concentration of the solute (provided $K^* = 0$). Moreover, as illustrated in Fig. 8(b), introducing the wall chemical reaction at either of the channel plates becomes evident, resulting in a notable reduction in the mean concentration. A gradual decline in the peak characterizes this, and overlapping of the mean concentration distribution is observed, similar to the result obtained by Das *et al.* [52]. Furthermore, the absorption of solute tracer particles at both channel boundaries results in a more rapid decrease in the mean concentration compared to other conditions. In Fig. 8(c), introducing bulk chemical reactions into the flow is observed to have a noticeable effect, as evidenced by a gradual decrease in the peak of the mean concentration distribution as the values of $K^*$ increase. Figure 8(d) shows that over time, the solute disperses more in the longitudinal direction, which

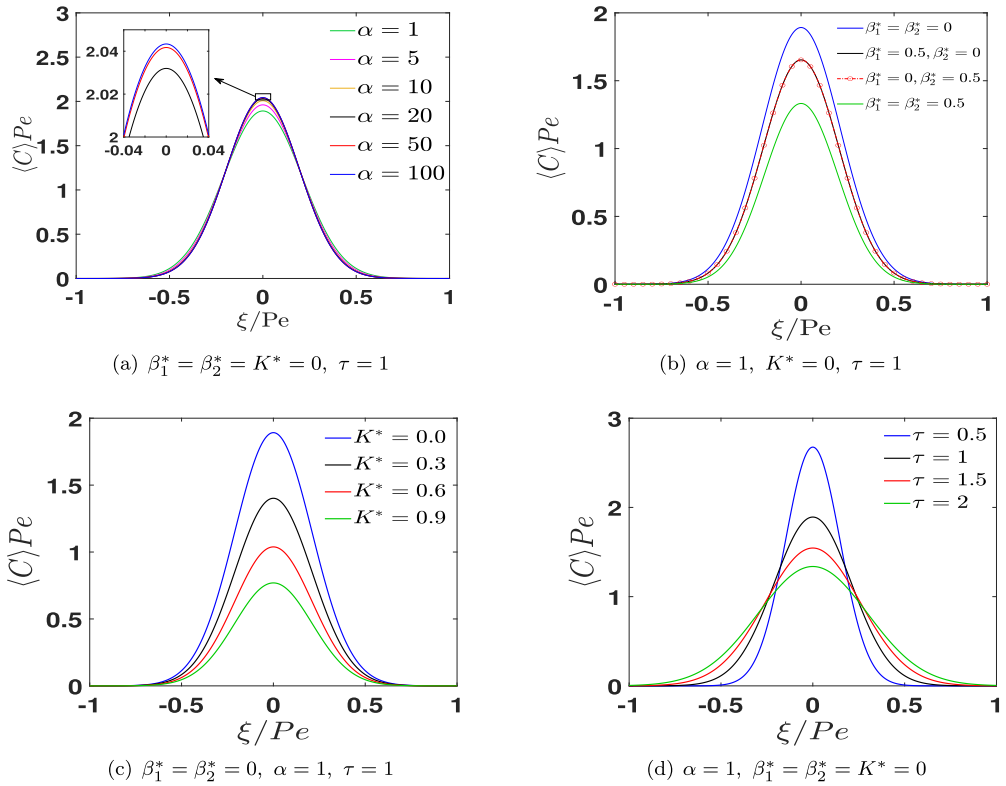


(a) $\beta_1^* = \beta_2^* = K^* = 0,\ \tau = 1$ (b) $\alpha = 1,\ K^* = 0,\ \tau = 1$

(c) $\beta_1^* = \beta_2^* = 0,\ \alpha = 1,\ \tau = 1$ (d) $\alpha = 1,\ \beta_1^* = \beta_2^* = K^* = 0$

FIG. 8. Mean concentration distribution for distinct (a) $\alpha$, (b) $\beta_1^*$ and $\beta_2^*$, (c) $K^*$, and (d) $\tau$.

causes the mean concentration profile to decrease. The solute molecules spread over time due to their continual movement and interactions with one another.

### E. Transverse concentration distribution

The asymptotic expansion in Eq. (20) can be used to derive the expression for two-dimensional concentration distribution up to the third order in a new coordinate system $\{\xi/\mathrm{Pe}, C\ \mathrm{Pe}\}$, in a similar way to how the mean concentration is derived, as

$$C\ \mathrm{Pe} = \frac{1}{\sqrt{4\pi {D_T}^* \tau}}\Bigg[1 + \frac{1}{2}(\beta_1^* + \beta_2^*)M + \frac{1}{4}(\beta_1^* + \beta_2^*)^2 Z + \frac{1}{8}(\beta_1^* + \beta_2^*)^3 S + \Bigg\{N + \frac{1}{2}(\beta_1^* + \beta_2^*)Y + \frac{1}{4}(\beta_1^* + \beta_2^*)^2 R\Bigg\}\frac{\partial}{\partial(\xi/\mathrm{Pe})} + \Bigg\{X + \frac{1}{2}(\beta_1^* + \beta_2^*)Q\Bigg\}\frac{\partial^2}{\partial(\xi/\mathrm{Pe})^2} + P\frac{\partial^2}{\partial(\xi/\mathrm{Pe})^3}\Bigg]$$
$$\times \exp\Bigg[-\frac{1}{4{D_T}^*\tau}\left(\frac{\xi}{\mathrm{Pe}}\right)^2 - \Bigg\{\frac{1}{2}(\beta_1^* + \beta_2^*) - \frac{1}{3}\left(\beta_1^{*2} + \beta_2^{*2} - \beta_1^*\beta_2^*\right) + K^*\Bigg\}\tau\Bigg]. \tag{78}$$

Figure 9 shows how the solute distribution along a channel flow varies over time, revealing a gradual shift from the zeroth order to the third order. At early times ($\tau < 1$), all three order terms contribute significantly to the concentration distribution. However, the higher-order terms become less significant in determining the distribution as time progresses. Hence, beyond $\tau = 1$, orders higher than the second order can be omitted and do not introduce significant inaccuracies, as observed from Fig. 9. Consequently, the graphical representations of the first-, second-, and

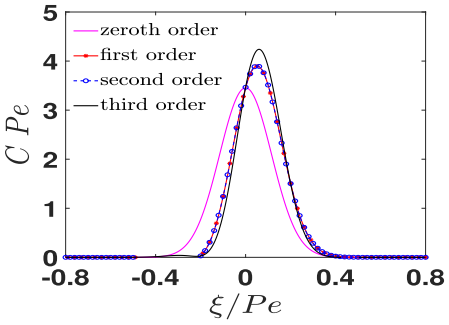


(a) $\tau = 0.3$

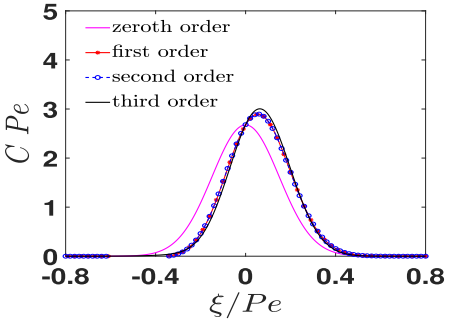


(b) $\tau = 0.5$

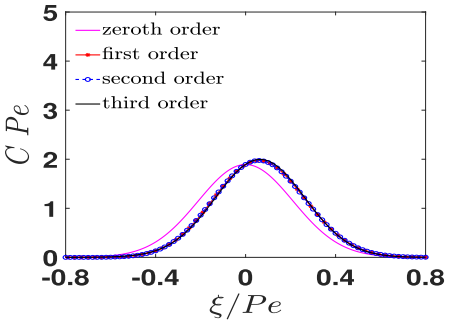


(c) $\tau = 1$

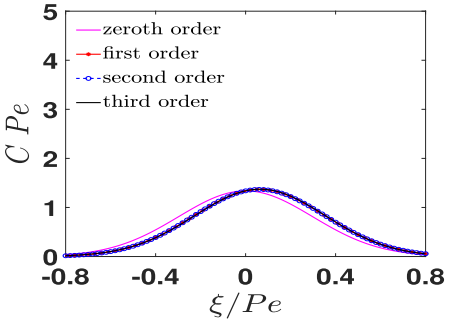


(d) $\tau = 2$

FIG. 9. Longitudinal distribution of transverse concentration derived as asymptotic expansions from zeroth to third order at different times, where $K^* = 0$, $\alpha = 1$, $\beta_1^* = \beta_2^* = 0$, and $y = 0$.

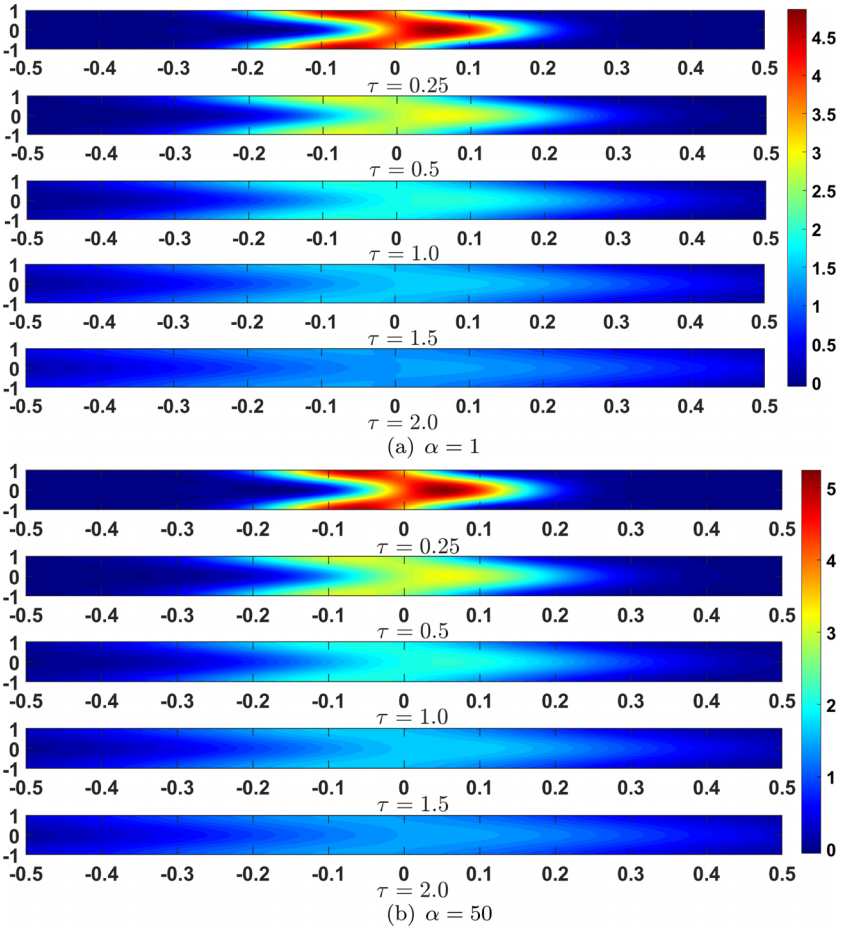


FIG. 10. Concentration contours for distinct $\tau$ in the absence of all chemical reactions (i.e., $\beta_1^* = \beta_2^* = 0$ and $K^* = 0$) (the horizontal axis indicates $\xi/\mathrm{Pe}$, and the vertical axis indicates $y$).

third-order approximations exhibit a remarkable similarity for $\tau > 1$. Hence, it might be adequate to determine approximate results only up to the second order.

The concentration contours in Figs. 10–15 provide an insight into the individual and combined effects of various parameters [such as the couple stress parameter ($\alpha$), the bulk chemical reaction parameter ($K^*$), and wall chemical reaction parameters ($\beta_1^*$ and $\beta_2^*$)] and also depict the influence of such parameters on the solute distribution phenomena. Initially, the solute is introduced at the $\xi = 0$ line and subsequently disperses throughout the channel due to the effect of advection, diffusion, and couple stress. The system coordinates in each case reflect the velocity, ensuring that the center of the concentration cloud consistently remains at the origin.

Figure 10 demonstrates the concentration distribution of the solute at various times for $\alpha = 1$ and 50 in the absence of bulk and wall chemical reactions. It is seen from Figs. 10(a) and 10(b) that from the source, the strength of the concentration tracer emerges near the channel centroid during the initial stage. Therefore both upstream and downstream regions exhibit a slight asymmetry in the concentration distribution at $\alpha = 1$ and 50. From this, it is clear that couple stress induces asymmetricity in the concentration distribution. Furthermore, lateral diffusion and advection induce the solute to move away from the channel centroid over time. Moreover, the advection becomes more dominant than diffusion as time progresses, which prompts the solute to spread more in

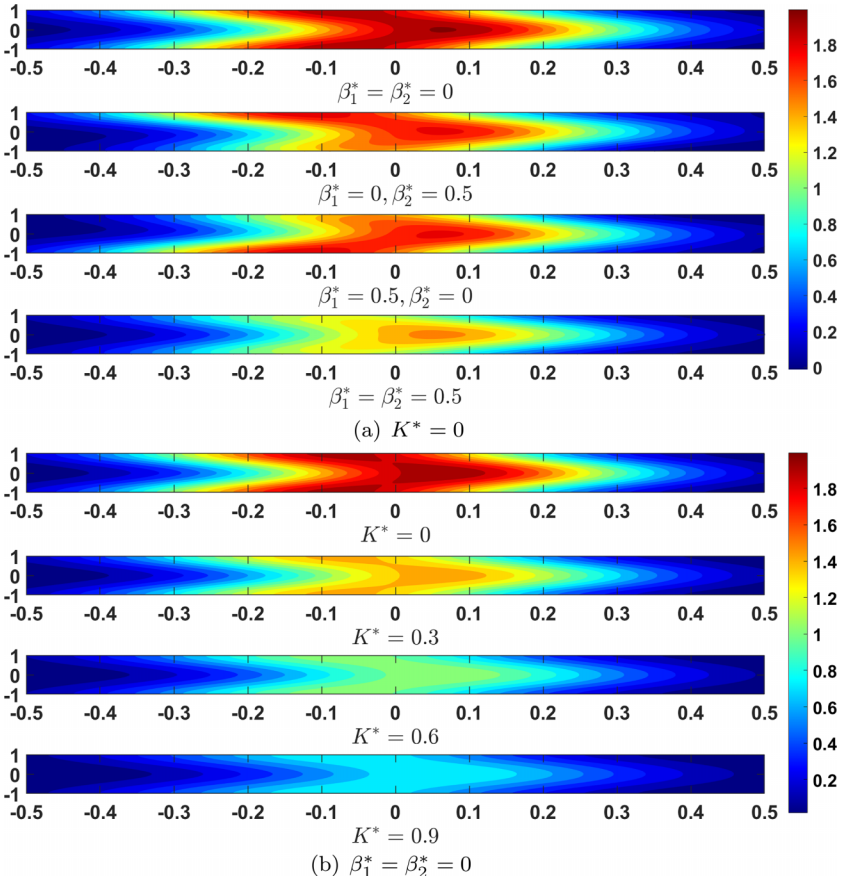


FIG. 11. Concentration contours with $\alpha = 1$ and $\tau = 1$ for different (a) $\beta_1^*$ and $\beta_2^*$ and (b) $K^*$.

the longitudinal direction. Consequently, the solute concentration decreases in both regions and becomes symmetric [49].

Figure 11 depict concentration contours for $\alpha = 1$ at $\tau = 1$, showcasing variations in $\beta_1^*$ and $\beta_2^*$ values, and in $K^*$ value, respectively. When there is no wall chemical reaction at the channel plates, the solute exhibits its highest concentration at the center of the channel rather than near the plates in both upstream and downstream locations. From Fig. 11(a), a decrease in solute concentration arises near the plates due to the influence of the wall chemical reactions. Moreover, asymmetry in the concentration distribution arises more in the upstream region because of the introduction of wall chemical reactions at either of the plates. Increasing the wall chemical reaction parameter at either of the channel plates decreases solute concentration near the absorption location, and the higher concentration zone becomes noticeable far away from the absorption location. In essence, the wall chemical reaction at either of the channel plates results in lower concentration at the boundary where it occurs and also introduces nonuniformity in the concentration distribution near the channel plates where it occurs. When the wall chemical reaction occurs at both channel plates without any bulk chemical reactions, we observe a region of lower concentration at both plates in contrast to the center of the channel. Moreover, the entire concentration in the channel subsequently decreased by increasing the wall chemical reaction at both channel plates. Figure 11(b) depicts the concentration contours related to distinct values of bulk chemical reaction parameters. Bulk chemical reactions are reactions that occur within the fluid itself. When we enhance the value of $K^*$, the solute concentration decreases across the entire channel uniformly, both upstream and downstream. This decline

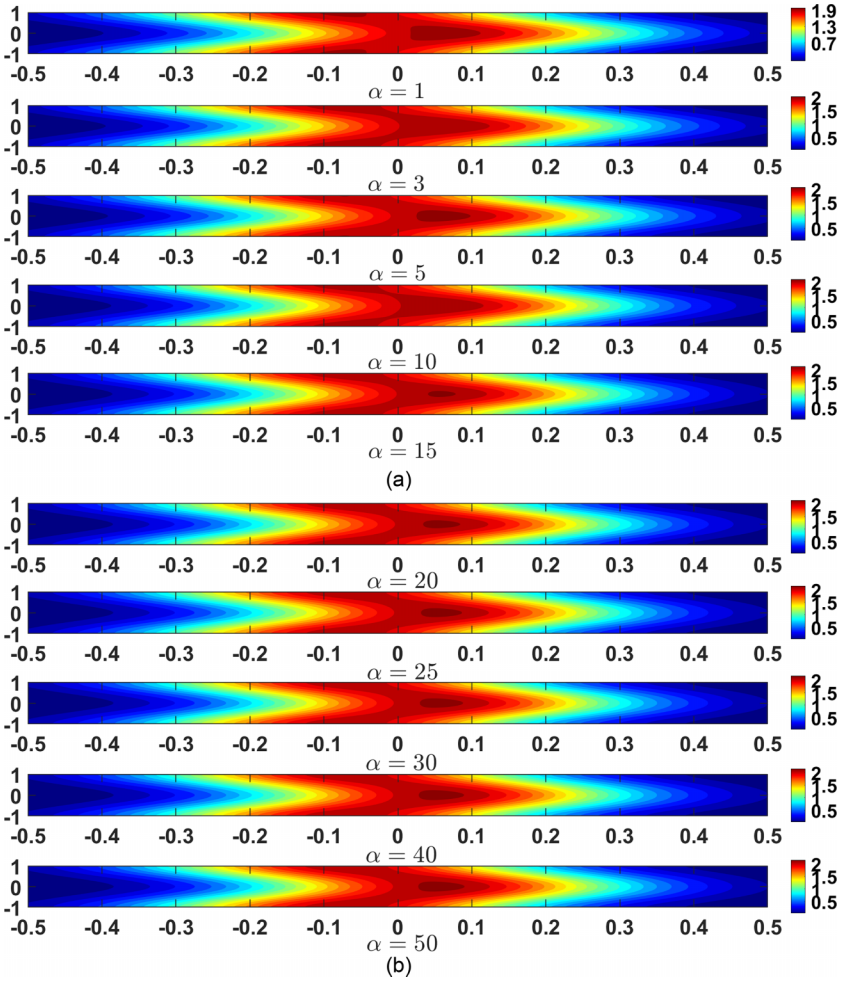


FIG. 12. Concentration contours for distinct values of $\alpha$ at $\tau = 1$ in the absence of bulk and wall chemical reactions (i.e., $K^* = 0$ and $\beta_1^* = \beta_2^* = 0$).

in solute concentration is because the bulk chemical reaction consumes the solute, leading to a decrease in solute concentration throughout the channel. The slight asymmetry of the concentration distribution in the channel is because of the couple stress parameter ($\alpha = 1$). Consequently, the slight asymmetry due to couple stress will gradually decrease by increasing the bulk chemical reaction.

Figures 12–15 expound the concentration contours of individual and combined effects of the couple stress and reaction parameters. It is seen from Figs. 12 and 13 that the concentration is significant without the influence of any reaction parameters for all values of $\alpha$. Introducing bulk and wall chemical reactions in the flow and at the plates, respectively, reduces the solute concentration throughout the channel for all $\alpha$. When no reactions are present, the solute concentration remains high for all values of the couple stress parameter $\alpha$, as the solute is transported primarily by advection and diffusion. However, when bulk reactions (within the fluid) and wall reactions (at the plates) are introduced, they actively consume or absorb the solute, reducing the channel's concentration. The reactions deplete the solute uniformly in the flow and at the boundaries (since we have fixed $\beta_1^* = \beta_2^* = 0.5$ at the plates), making their impact noticeable for all values of $\alpha$,

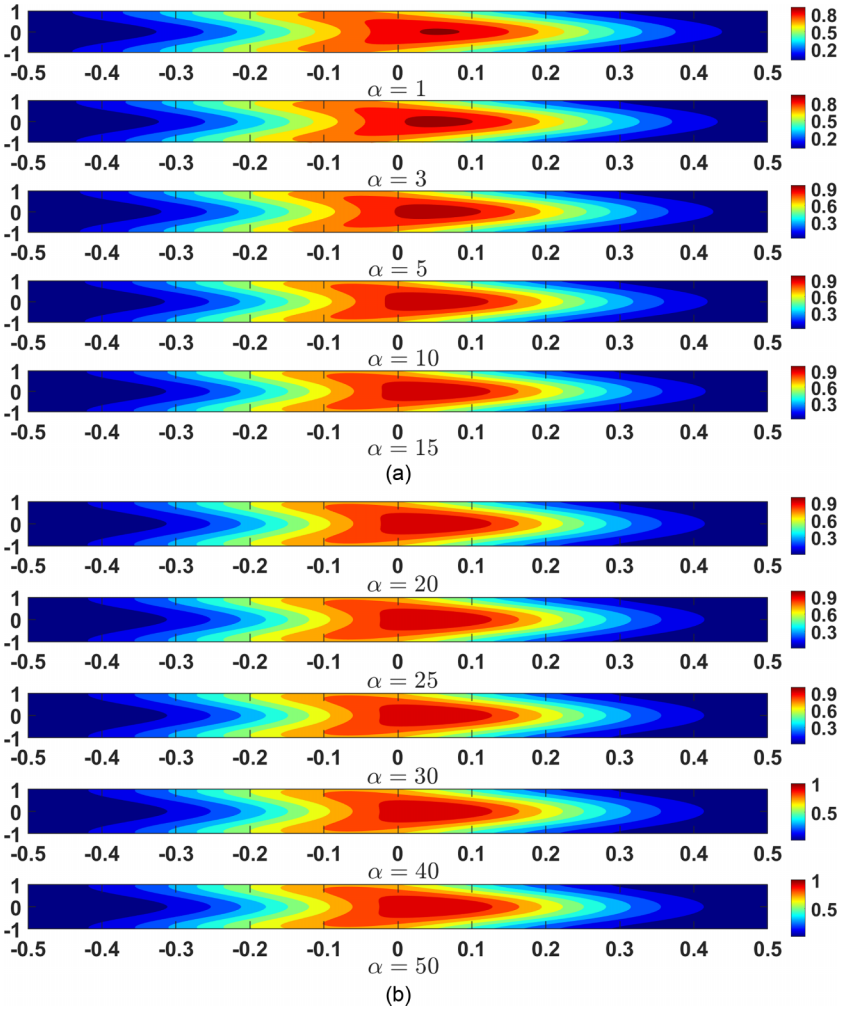


FIG. 13. Concentration contours for distinct $\alpha$ at $\tau = 1$ with $\beta_1^* = \beta_2^* = 0.5$ and $K^* = 0.5$.

regardless of the couple stress effects. For example, in drug delivery systems or chemical reactors, introducing bulk and wall reactions can be an effective way to precisely control the concentration of active substances across the flow, allowing for targeted reactions or substance depletion in specific regions of the device.

Figures 14 and 15 visualize the individual effects of the chemical reactions with the couple stress effect. It is evident from Fig. 14 that wall chemical reactions at the plates have reduced the solute concentration near the plates, leading to a higher concentration of solute accumulation at the center of the channel's cross section. Notably, the concentration is less for smaller values of $\alpha$ when compared to larger values of $\alpha$. In other words, by increasing the $\alpha$ values, the solute concentration of the channel increases. Moreover, the concentration near the plates is reduced due to wall chemical reactions, prompting diffusion to transport solute molecules away from the regions near the plates. However, due to potentially less influence of the wall chemical reaction in the center of the channel, diffusion becomes relatively less affected by the wall chemical reactions occurring at the plates. As a result, the solute molecules tend to accumulate more in the center, leading to a higher concentration in the center than elsewhere in the channel for increasing values of $\alpha$. Introducing bulk chemical

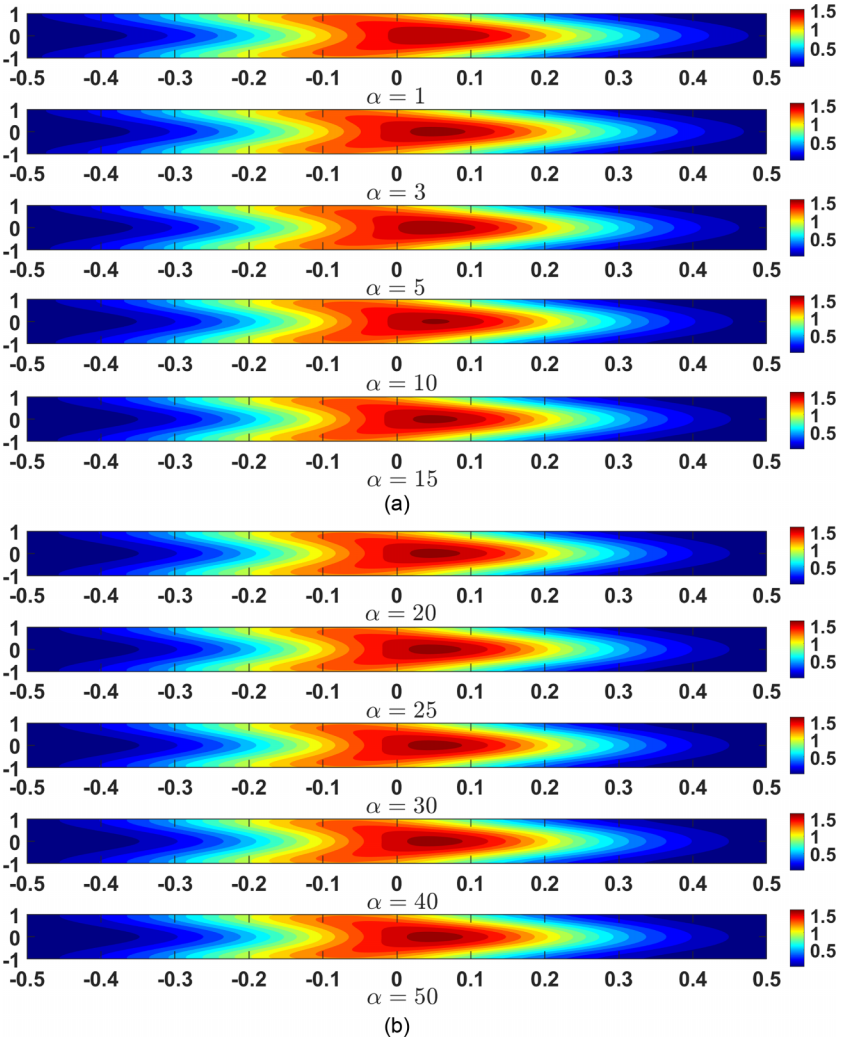


FIG. 14. Concentration contours for distinct $\alpha$ with $\beta_1^* = \beta_2^* = 0.5$ and $K^* = 0$.

reactions in the channel flow uniformly decreases the concentration of the solute throughout the channel. In comparing the individual effects of the bulk and wall chemical reactions, it becomes apparent that bulk chemical reactions notably decrease solute concentration compared with wall chemical reactions (see Fig. 15).

Figure 16 presents the concentration distribution at different distances from the boundary $y = -1$, with a specific focus on the mean concentration distribution under various combinations of $\beta_1^*$ and $\beta_2^*$ at a dispersion time of $\tau = 1.0$. When there is no wall chemical reaction the concentration is governed solely by advection and diffusion. Due to the high velocity at the center, the fluid flows more rapidly at ($y = 0$), causing the solute to be advected more efficiently downstream. Although advection primarily transports the solute along the flow direction, the transverse diffusion is less at the center due to the solute being carried by the flow. In other words, faster advection at the center of the channel reduces transverse diffusion and keeps the solute concentrated in the region, leading to higher concentration at the center of the channel $y = 0$. Between the walls and the center, particularly at $y = \pm 0.5$ the fluid velocity is not fast enough to advect solute as efficiently

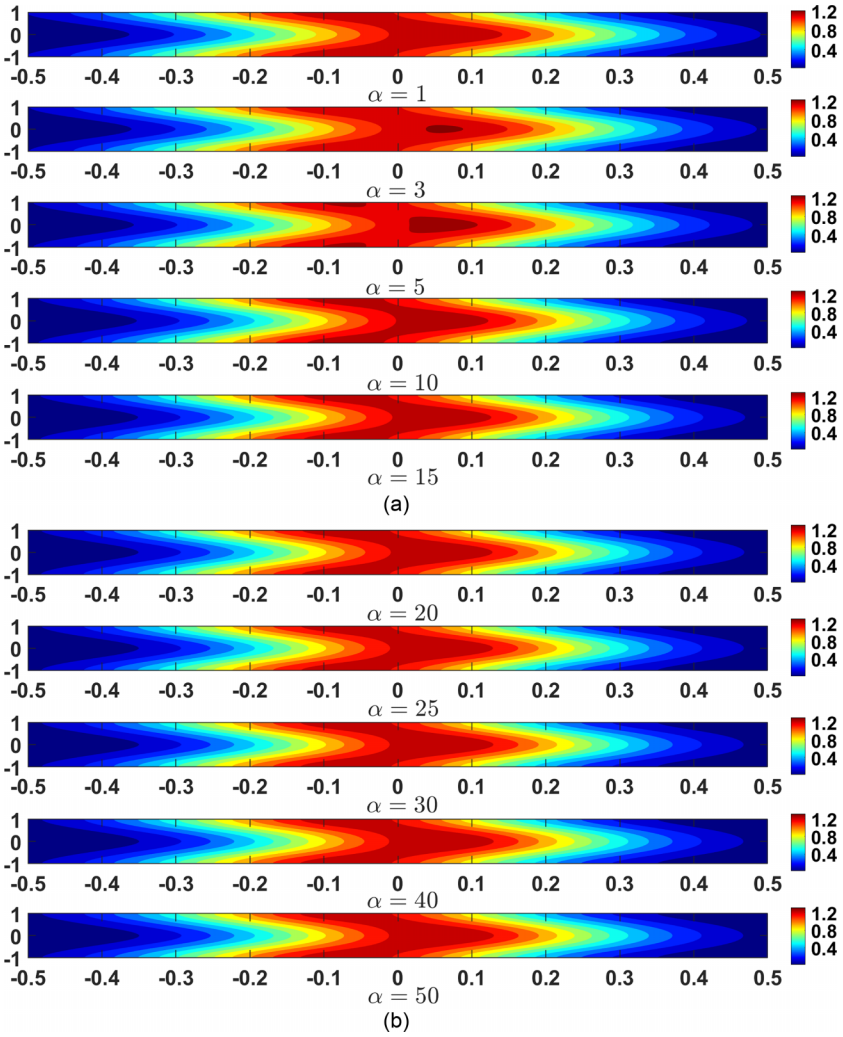


FIG. 15. Concentration contours for distinct $\alpha$ at $\tau = 1$ with $\beta_1^* = \beta_2^* = 0$ and $K^* = 0.5$.

as in the center, and diffusion spreads the solute more evenly, leading to lower concentrations. Therefore when there is no wall chemical reaction at either boundary, the solute concentration is highest at the center of the channel ($y = 0$) and lowest at $y = \pm 0.5$. The concentration curves in the upstream region at $y = 1$ coincide with $y = -1$ and similarly $y = 0.5$ coincides with $y = -0.5$ due to the symmetry nature of the flow, and the peak of the mean concentration curve is close to the maximum concentration curve at $y \pm 0.5$. When a wall chemical reaction is introduced on either the upper or lower plate, it absorbs the solute near that boundary. As a result, solute concentrations near the reacting plate are reduced. Figures 16(b) and 16(c) reveal that imposing wall chemical reactions on the upper or lower plate impacts the concentration curves near the plate to move in the downstream region because of the reaction rate influencing solute concentration along the flow direction, resulting in lower concentrations near the plate and causing the solute to migrate downstream. The concentration far away from the plate shifts toward the upstream region because the lack of significant chemical reactions in these regions allows the solute to remain largely unaffected, preserving its distribution upstream. It is noted that introducing the same level

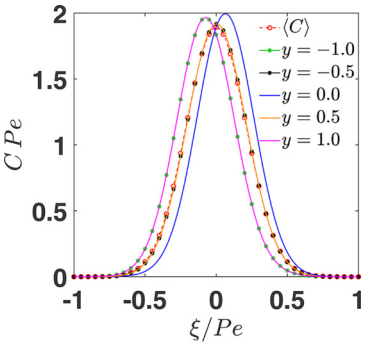


(a) $\beta_1^* = \beta_2^* = 0$

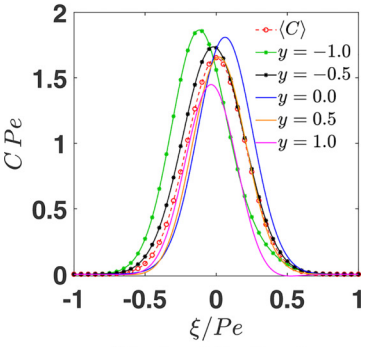


(b) $\beta_1^* = 0.5,\ \beta_2^* = 0$

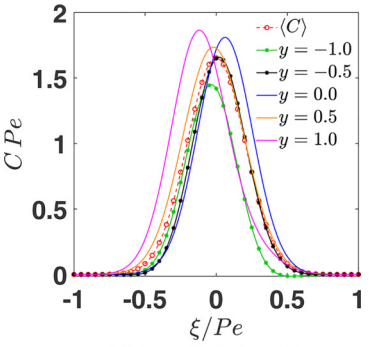


(c) $\beta_1^* = 0,\ \beta_2^* = 0.5$

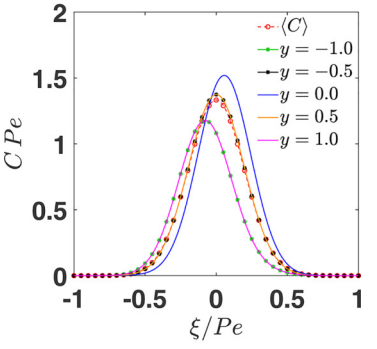


(d) $\beta_1^* = 0.5,\ \beta_2^* = 0.5$

FIG. 16. Concentration distribution at different widths for different combinations of $\beta_1^*$ and $\beta_2^*$ with $\tau = 1$, $\alpha = 1$, and $K^* = 0$.

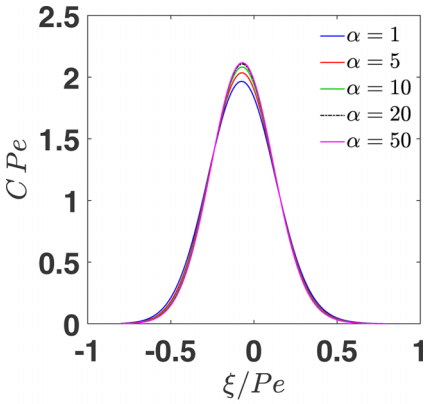


(a) $y = \pm 1$

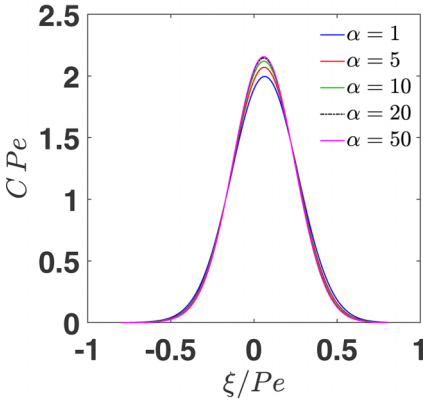


(b) $y = 0$

FIG. 17. Transverse concentration distribution for different $\alpha$, where $\tau = 1$, $K^* = 0$, and $\beta_1^* = \beta_2^* = 0$.

of reactions on both plates leads to coinciding concentration curves at $y = \pm 1$ and similarly at $y = \pm 0.5$ because the chemical reactions are uniformly impacting both boundaries, leading to a balanced distribution of solute across the channel. Also, the concentration profile at $y = \pm 0.5$ tends to approach the mean concentration [see Fig. 16(d)]. In other words, introducing the wall chemical reaction in all the analyzed scenarios results in a uniform reduction in the transverse concentration profiles.

Figure 17 displays the impact of $\alpha$ on the transverse concentration distribution with no other reactions imposed at varying distances from the lower plate of the channel ($y = -1$). The longitudinal profile of transverse concentration for different values of $\alpha$ demonstrates that for $\alpha \geqslant 20$, the dispersion is less due to the negligible effect of couple stress, resulting in a high concentration. And for $\alpha < 20$ due to high couple stress, the concentration curve decreases. At $y = \pm 1$, diffusion causes the solute concentration peak to move upstream, whereas, at $y = 0$, advection leads to its downstream shift. Remarkably, an intriguing observation is the subtle increase in concentration, particularly noticeable at higher $\alpha$ values. For instance, at $\alpha = 50$, $C$ Pe is 2.1166, but drops to 2.1066 at $\alpha = 20$. Figure 17 illustrates this trend. Also, it is noted that the transverse concentration becomes more appropriate than the mean concentration.

Figure 18 showcases the impact of reaction parameters in transverse concentration distribution. When, $\alpha = 1$ the couple stress is high, resulting in increased dispersion, which leads to a lower transverse concentration. In contrast, at $\alpha = 50$, the couple stress effect diminishes, reducing dispersion and thereby increasing the transverse concentration. The figures show that in the absence of reaction

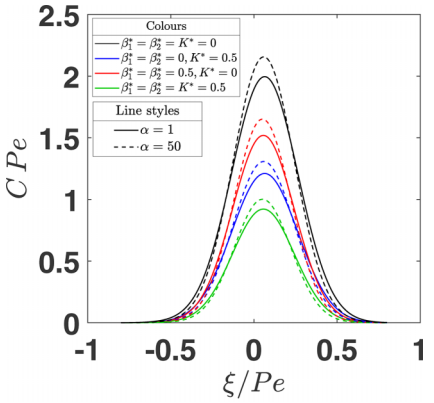


(a) $y = 0$

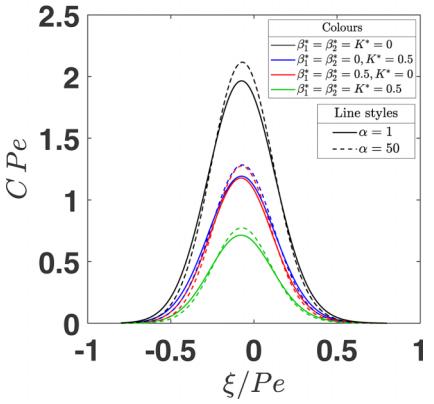


(b) $y = \pm 1.0$

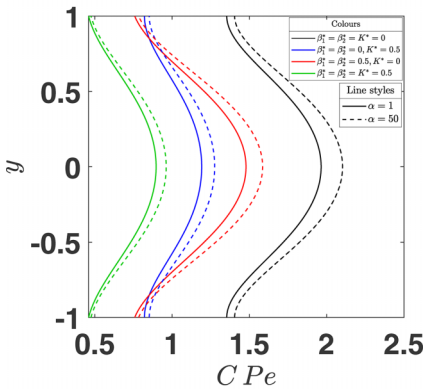


(c) $\xi/Pe = 0.1$

FIG. 18. Transverse concentration distribution for distinct reactions at $\tau = 1$.

parameters, the transverse concentration is significantly higher than in other scenarios, as the solute transport relies solely on advection and diffusion. Furthermore, the transverse concentration is higher at the center of the channel ($y = 0$) compared to near the center, e.g., $y = \pm 0.5$, and at the plates ($y = \pm 1$) because the rapid fluid flow at the center effectively transports solute, minimizing the influence of diffusion. This efficient transport at the channel center leads to a higher solute concentration. Since the reactions are absent and solute distribution is governed only by flow

dynamics and diffusion, the solute spreads more evenly and has an upstream shift in the peak concentration. However, when reactions are present, they reduce the transverse concentration profile for $\alpha = 1$ and 50. Near the center ($y = \pm 0.5$) and at $y = \pm 1$, increased shear and wall reactions further decrease solute concentration. Wall chemical reactions at the channel boundaries absorb solute, reducing concentration at the plates and shifting the peak concentration upstream from the center. Notably, Fig. 18(c) reveals that at the center of the channel's cross section and the region near the center, the bulk chemical reactions are more effective in reducing the transverse concentration profile compared to the wall chemical reaction, particularly for smaller values of $\alpha$ where the couple stress is significantly high. However, at the channel plates, an upside-down characteristic can be observed because, at the channel plates, the wall chemical reactions are more effective in reducing the concentration of the solute than the bulk chemical reactions.

For a more accurate analysis of the effect of reaction parameters and $\alpha$, it is crucial to investigate the variations in the transverse concentration distribution beyond the mean concentration. An indicator denoted as $C_v$ is being used [32,38,39] in the following manner:

$$C_v(\xi, \tau) = \max_{(-1 \leqslant y \leqslant 1)} C(\xi, y, \tau) - \min_{(-1 \leqslant y \leqslant 1)} C(\xi, y, \tau) \tag{79}$$

where it is defined as the difference between the maximum and minimum solute concentrations at any given longitudinal position. This function represents the transverse variation across the channel cross section. Its primary role is to explore how the parameters $\alpha$, $K^*$, $\beta_1^*$, and $\beta_2^*$ affect the uniformity and nonuniformity of solute transverse concentration. The subsequent paragraph delves into the longitudinal distribution of transverse variation in solute concentration, as shown in Figs. 19–22. It shows how the transverse variation changes as the solute cloud flows longitudinally from the origin, with concentration variation increasing from zero to maximum.

Figures 19(a)–19(c) portray how transverse variations in solute concentration evolve with different dispersion times. The graph in Fig. 19(a) represents the longitudinal dispersion of the solute concentration's transverse variation in a scenario where wall chemical reactions are absent. As time progresses, the peak transverse concentration variation diminishes in upstream and downstream regions. The transverse variation is slightly asymmetric about the centroid of the solute cloud because the high concentration zone of the solute is always seen in the downstream region, which enhances more concentration variation in the downstream region for all values of $\alpha$ [see Figs. 10(a) and 10(b)] and exhibits a bimodal distribution. But at a considerable time [$\tau \sim O(10)$], the variation becomes uniform [see Fig. 19(a)] for all values of $\alpha$. This characteristic is similar to the result obtained by Wu and Chen [38,39]. Figure 19(b) shows the longitudinal distribution of the transverse variation in solute concentration for cases with wall chemical reactions at either of the plates. In these cases, the peak concentration variation diminishes as the solute cloud moves away from its centroid over time. However, the upstream region exhibits the most significant concentration variation when the reaction occurs at either of the plates [59]. Referring to Fig. 11(a), which depicts the higher concentration zone in the upstream location at either of the plates where the wall chemical reaction has not occurred, the concentration variation is high upstream. But from Fig. 19(b) we observe, as time progresses, e.g., $\tau > 10$, that the variation diminishes, leading to the transition from a bimodal to a unimodal distribution. Figure 19(c) shows the longitudinal distribution of the transverse variation in solute concentration for a case with wall chemical reactions employed at both boundaries. As the solute cloud flows downstream, it disperses more, resulting in a significant transverse variation of solute concentration in the downstream region. Over time ($\tau > 10$), the wall chemical reaction at the plates tends to smooth out the transverse variation in solute concentration, resulting in a transition from a bimodal to a unimodal distribution.

Figure 20 reveals the impact of wall chemical reactions with $\alpha = 1$ in the absence of the bulk chemical reaction. The figure clearly shows that applying the wall chemical reaction to either of the channel plates reveals high nonuniformity. Furthermore, an increase in wall chemical reaction at either of the plates causes the variation curves to shift toward an unimodal distribution, with a higher concentration variation in the upstream region because the concentration starts to smooth out

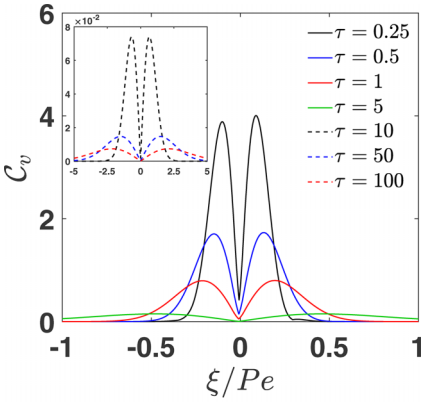


(a) $\beta_1^* = \beta_2^* = 0$

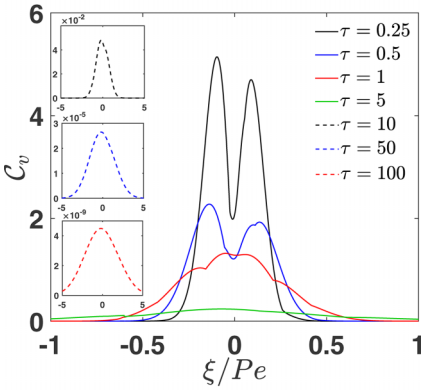


(b) $\beta_1^* = 0.5,\ \beta_2^* = 0$ (or, $\beta_1^* = 0,\ \beta_2^* = 0.5$)

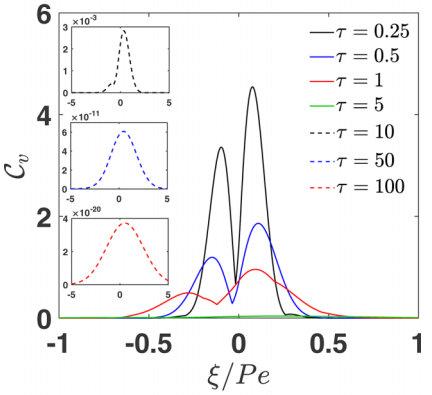


(c) $\beta_1^* = \beta_2^* = 0.5$

FIG. 19. Longitudinal distribution of transverse concentration variation with various wall chemical reactions at different times ($\tau$) when $K^* = 0$ and $\alpha = 1$.

in the downstream location. The maximum concentration is present only in the upstream location [see Fig. 11(a)]. Introducing the same rate of wall chemical reaction on both plates results in the concentration variation peak moving downstream, with an initial peak observed upstream. However, this peak deteriorates as the wall chemical reaction intensifies equally on both plates.

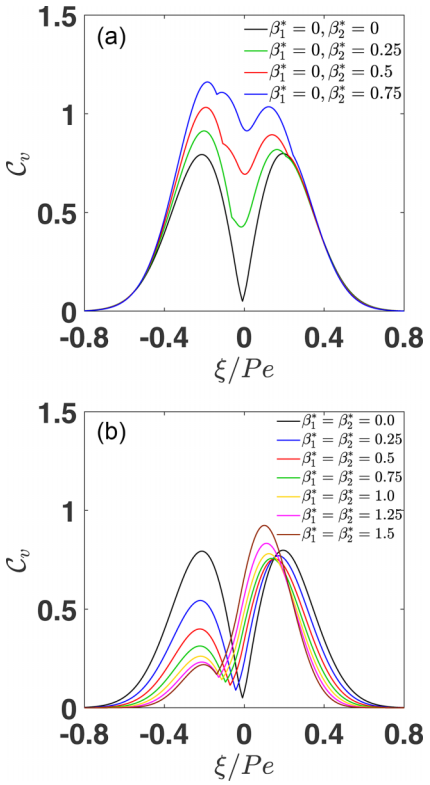


FIG. 20. Longitudinal profile of transverse concentration variation with various wall chemical reactions with $\alpha = 1$ and $K^* = 0$ at $\tau = 1$.

Figure 21 displays the longitudinal evolution of transverse concentration variation for different values of $\alpha$ in combination with various wall chemical reactions. A clear pattern emerges from Figs. 21(a)–21(c) that changes in $\alpha$ result in comparable variation in transverse concentration distribution further affecting the uniformity in the transverse variation and peak variation across the flow domain. In the absence of reaction parameters, the transverse concentration variation increases for increasing $\alpha$ at $\tau = 1$ with slight nonuniformity. This is due to the higher concentration in the downstream region than in the upstream region (see Fig. 12). But as time progresses this subtle nonuniformity diminishes, leading to a uniform increase in the transverse concentration variation. Notably, for $\alpha \geqslant 20$ the increase in transverse concentration variation is subtle due to the predominance of low couple stress and diffusion. In contrast, the diffusion is maximum for $\alpha < 20$ where the couple stress is dominant, resulting in a decrease in the concentration variation. The concentration variations for different $\alpha$ values when the wall chemical reactions occur on either of the channel plates are shown in Fig. 21(b). Suppose the wall chemical reaction occurs on either or both plates of the channel; it is observed that increasing $\alpha$ increases the transverse concentration variation with significant nonuniformity. The highest concentration variation is observed upstream when the wall chemical reaction occurs on either of the channel plates. This is because as the solute moves downstream, the reaction at either of the walls absorbs the solute, causing variation in the concentration profile near the walls, and resulting in a pronounced concentration variation in the upstream region [see Fig. 11(a)]. From Fig. 21(c), it is seen that the downstream region displays the most notable concentration variation when wall chemical reactions happen equally on both boundaries. However, the concentration variation gradually diminishes by decreasing $\alpha$ and contributes to the transition from bimodal to unimodal over time. Moreover, the significant

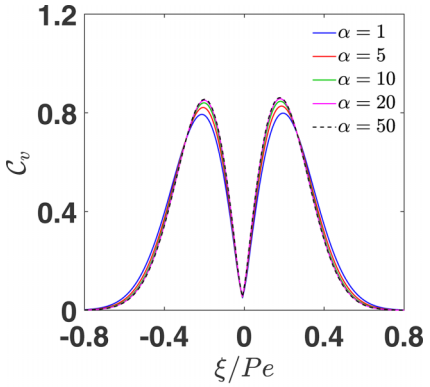


(a) $\beta_1^* = \beta_2^* = 0$

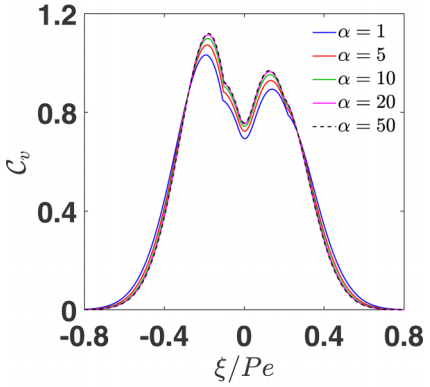


(b) $\beta_1^* = 0.5,\ \beta_2^* = 0$ (or, $\beta_1^* = 0,\ \beta_2^* = 0.5$)

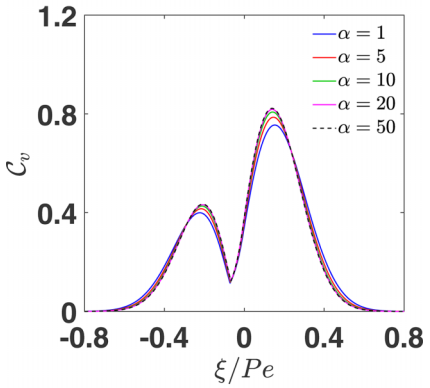


(c) $\beta_1^* = \beta_2^* = 0.5$

FIG. 21. Longitudinal profile of transverse concentration variation with various wall chemical reactions and different $\alpha$ values, at $K^* = 0$ and $\tau = 1$.

nonuniformity in the transverse concentration variation is only due to the presence of the wall chemical reaction for all values of $\alpha$.

Since the difference in maximum values of concentration variation present in the upstream and downstream regions is very subtle at $\tau = 1$, the maximum concentration variation found in the upstream and downstream regions is presented in Table IV to showcase the nonuniformity in the concentration variation.

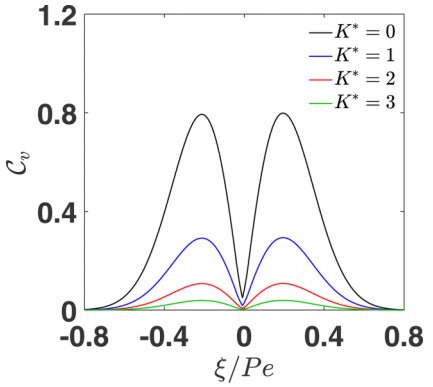


(a) $\beta_1^* = \beta_2^* = 0$

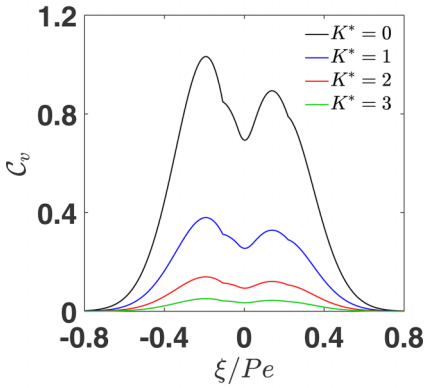


(b) $\beta_1^* = 0.5,\ \beta_2^* = 0$ (or, $\beta_1^* = 0,\ \beta_2^* = 0.5$)

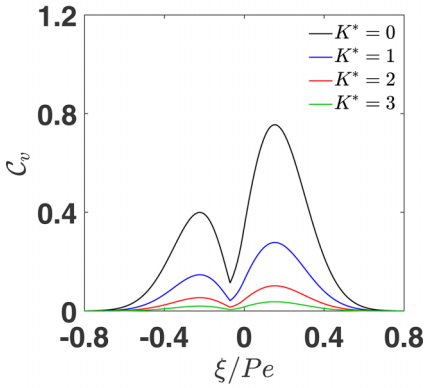


(c) $\beta_1^* = \beta_2^* = 0.5$

FIG. 22. Longitudinal profile of transverse concentration variation with various wall chemical reactions for distinct bulk chemical reaction conditions with $\alpha = 1$ and $\tau = 1$.

TABLE IV. Concentration variation for distinct $\alpha$ values when $\tau = 1$, $K^* = 0$, and $\beta_1^* = \beta_2^* = 0$.

| $\alpha$ | 1 | 5 | 10 | 20 | 50 |
|---|---|---|---|---|---|
| Upstream | 0.7935 | 0.8214 | 0.8405 | 0.8506 | 0.8547 |
| Downstream | 0.7986 | 0.8273 | 0.8468 | 0.8571 | 0.8612 |

TABLE V. Concentration variation for distinct $K^*$ values when $\alpha = 1$, $\tau = 1$, and $\beta_1^* = \beta_2^* = 0$.

| $K^*$ | 0 | 1 | 2 | 3 |
|---|---|---|---|---|
| Upstream | 0.7935 | 0.2919 | 0.1074 | 0.0395 |
| Downstream | 0.7986 | 0.2938 | 0.1081 | 0.0398 |

Table IV ensures the nonuniformity of the concentration variation for all values of $\alpha$. However, this nonuniformity in concentration variation is due to couple stress. The table also shows that as $\alpha$ increases, the nonuniformity in transverse concentration variation increases.

Figures 22(a)–22(c) illustrate how bulk chemical reaction affects the longitudinal distribution of transverse concentration variation for the distinct values of the wall chemical reactions. In the absence of a wall chemical reaction, as illustrated in Fig. 22(a), the increase in bulk chemical reaction parameter decreases the variation in transverse concentration. However, a very slight asymmetry in the variation is observed which is because of $\alpha$ where $\tau = 1$. It is evident from Fig. 15 that the transverse concentration is slightly high in the downstream when compared with the upstream region, leading to the slight nonuniformity in the concentration variation for different values of $K^*$. Although this slight nonuniformity is present for a small value of $K^*$, it deteriorates for large $K^*$ and eventually becomes uniform throughout the entire stream. As seen in Figs. 22(b) and 22(c), the nonuniformity in transverse concentration variation is caused by the wall chemical reaction parameters and the couple stress parameter $\alpha$. The wall chemical reaction at the plates reacts with solute molecules, leading to the higher concentration of the solute at the center of the channel cross section (see Fig. 13). This higher concentration of solute in the center of the cloud leads to a nonuniform transverse variation. Notably, the bulk chemical reaction does not cause any nonuniformity in the transverse concentration variation. The significant nonuniformity observed in transverse variation is solely because of the wall chemical reaction.

As the difference in peak concentration values between the upstream and downstream regions is subtle, Table V displays the maximum concentration variation in these regions to illustrate the nonuniformity in concentration variation for various values of $K^*$.

Table V showcases that the nonuniformity in concentration variation decreases as $K^*$ increases. However, for a large value of $K^*$, the subtle nonuniformity in transverse concentration variation vanishes and the transverse concentration variation becomes uniform throughout the entire stream.

Figures 19–22 illustrate the transverse concentration variations concerning time, couple stress, wall reactions, and bulk chemical reactions. Notably, all the profiles exhibit double peaks in the transverse concentration variation. These double peaks result from the interplay of flow dynamics and diffusion across the channel. As the solute is transported, concentration variations arise due to differences in flow velocity and boundary effects. The higher flow velocity near the channel center, combined with the no-slip condition at the walls, creates regions of maximum and minimum transverse concentration. Although the solute primarily moves downstream, diffusion causes some of it to spread upstream, forming a concentration gradient and resulting in a peak in the transverse concentration variation. Similarly, downstream advection, combined with transverse diffusion, generates another gradient, leading to a second peak. Thus, the double peaks arise from the combined effects of advection and diffusion, which create concentration gradients on both sides of the solute source. The persistence or diminishing of these peaks over time depends on the presence and strength of wall chemical reactions, emphasizing the integrated influence of advection, diffusion, and reaction processes on solute behavior.

## VI. APPLICATIONS IN ADVANCING MICROFLUIDIC SYSTEMS

The exploration of how couple stress influences the longitudinal dispersion of a soluble substance undergoing molecular diffusion in the flow of a viscous fluid within horizontal channels is a

burgeoning area of research that holds great promise for various applications, including microfluidic devices, environmental engineering, and food engineering, among others. Couple stress is a fundamental fluid property, so understanding the influence of couple stress in the context of flow within rectangular channels is of utmost importance. Numerous scientific and engineering domains, including microscale material modeling, utilize the concept of couple stress. It plays a significant role in advancing the design and performance of microfluidic devices, enhancing the separation of fluids and components, improving fluid mixing, and broadening the comprehension of fluid flow phenomena in a more general sense. It has a wide range of applications, such as chemical synthesis, drug delivery and diagnostic assays, and the analysis of complex microscale systems like microelectromechanical and nanomaterial systems. It is evident from Figs. 12 and 13 that the significant values of $\alpha$ have greater implications in terms of application. These figures demonstrate how varying couple stress influences fluid flow and solute dispersion, which is critical for optimizing drug delivery systems and enhancing mixing efficiency in microfluidic devices. By leveraging these insights, engineers can design more effective biomedical applications, ensuring precise control over flow characteristics and improved performance in real-world scenarios. At very large $\alpha$, where couple stress is negligible, the flow resembles Poiseuille flow, typical of fluids with minimal microstructural influence. This leads to consistent concentration profiles and efficient transport, making it ideal for applications like drug delivery or reagent mixing in microfluidic devices [60]. In high-viscosity industrial processes, where dispersion is primarily driven by viscosity, a higher $\alpha$ ensures more controlled and predictable flow, which benefits drug release systems. As $\alpha$ decreases, couple stress effects increase, leading to higher dispersion, which spreads the solute more and results in a lower concentration distribution. Strong couple stresses (small $\alpha$) are particularly important in microfluidics because they directly impact fluid behavior, flow control, device performance, and the protection of sensitive materials. Understanding these effects is crucial for designing reliable, high-precision systems in various real-world applications. In highly concentrated suspensions or polymer solutions [53], such as chemical reactors or complex fluid processing, high couple stress can cause extensive mixing and dispersion, potentially lowering reactant or product concentrations in certain regions, which may affect process efficiency. For example, in laboratory-on-a-chip devices used for personalized medicine, understanding how large molecules like proteins or antibodies behave under couple stresses ensures accurate detection and analysis, improving diagnostic outcomes. In drug delivery systems, couple stress influences drug mixing and transport, affecting release rates and efficacy. Similarly, in cell sorting devices, a lower $\alpha$ may improve the separation of cells based on their physical characteristics.

## VII. CONCLUSION

This paper utilized a multiscale homogenization technique to investigate how solute concentration disperses within a two-dimensional viscous, couple stress fluid flowing between parallel plates. This system incorporates wall chemical reactions on both plates and introduces a bulk chemical reaction into the fluid flow. This research offers a profound insight into the impact of couple stress on the dispersion of solute concentration, enabling a comprehensive understanding of this phenomenon. An analytical solution is obtained for the two-dimensional concentration transport of solute using homogenization for multiple scales that effectively determines the dispersion coefficient, mean concentration, and transverse concentration distributions up to three orders. We examined the dispersion coefficient compared to prior research and observed an exact match to the findings of Rudraiah *et al.* [23] and Soundalgekar [20] regarding the impact of $\alpha$ on dispersion. Furthermore, we use an indicator to ascertain variations in transverse concentration. This paper yields the following significant results.

(1) The dispersion coefficient has a subtle decrease for $\alpha \gg 20$ due to dominant viscosity and the negligible couple stress. However, for $\alpha \ll 20$, there is a rapid decrease in the dispersion coefficient due to the strong effect of couple stress.

(2) The dispersion for $\alpha \ll 1$, in particular, when $\alpha \to 0$ exhibits inconsistent behavior because of unexpected interactions and distributions, driven up by the intricate relation of viscosity and couple stress, can be considered as a limitation.

(3) Increasing the parameters of wall chemical reactions results in reduced solute dispersion for all values of $\alpha$. This occurs because more intense wall reactions effectively remove (i.e., absorb) solute molecules from the region near the wall, thus restricting the overall dispersion of the solute.

(4) Mean concentration increases with increasing $\alpha$. Interestingly, for $\alpha \geqslant 20$ with less couple stress effect, there is a slight increase in mean concentration, while for $\alpha < 20$, the mean concentration decreases with amplification in the longitudinal dispersion due to the dominant effect of couple stress.

(5) The introduction of a wall chemical reaction at one or both boundaries results in a decrease in the transverse concentration profile. Also, applying these reactions to one of the channel plates results in overlapping characteristics of transverse concentration distribution at the center of the channel width.

(6) Bulk chemical reaction reduces the transverse concentration of the solute more effectively than the wall chemical reactions; specifically it is more efficient for smaller $\alpha$ values where the couple stress is more significant.

(7) For smaller values of $\alpha$, the concentration contour exhibits a reduction in concentration distribution, while larger values of $\alpha$ yield a subtle increase in concentration. Moreover, for varying $\alpha$, the concentration contour displays a slight asymmetric profile due to the influence of couple stress.

(8) In the channel's center, bulk reactions are more effective than wall reactions in reducing transverse concentration profiles, especially for small $\alpha$ with high couple stress, but at the channel plates an inverted characteristic is noticeable.

(9) In the absence of wall chemical reactions, transverse concentration variation diminishes and remains uniformly distributed around the channel centroid for an extended period. Introducing wall chemical reactions shifts the variation from bimodal to unimodal. When wall chemical reactions occur on either plate, concentration variation increases upstream due to diffusion's dominance over couple stress. Furthermore, when the reaction occurs on both plates, a significant nonuniformity emerges in transverse concentration, particularly downstream.

(10) As the bulk chemical reaction rate increases without wall chemical reactions, the transverse variation in concentration distribution decreases uniformly. Conversely, introducing the wall chemical reactions results in high nonuniformity, even when large values of $K^*$ are considered.

(11) The bulk chemical reaction has less impact on the nonuniformity of the transverse concentration variation. However, couple stress exhibits greater efficacy in the nonuniformity of the concentration variation for distinct values of $K^*$. Interestingly, the couple stress parameter and the wall chemical reaction parameters significantly impact concentration variation.

In this paper, we have investigated the dynamics of couple stress fluid flow, focusing on its behavior in the presence of the irreversible wall and bulk chemical reactions. Employing a multiscale homogenization technique, we have unraveled the intricate interplay of these phenomena. In future endeavors, this paper can be expanded to elucidate phase exchange kinetics by incorporating reversible reactions [32,61] and exploring the impact of nonlinear chemical reactions to enhance model accuracy, gain deeper insights into reaction mechanisms, and improve applicability to real-world systems. Also, we can extend this paper by focusing on non-Newtonian fluids where the couple stress effects capture the complex rheological behavior of fluids with internal microstructures. Future research could explore the application of the multiscale method to study couple stress fluid flow in a linearly permeable rectangular channel within a Darcy porous medium. This approach may be beneficial for investigating blood flow in arteries, particularly those with defects, and offer an effective way to reduce blood flow, lower blood pressure, and address related cardiovascular diseases [62,63].

**ACKNOWLEDGMENTS**

The authors wish to express their sincere thanks to the Chief Editor, Associate Editor, and anonymous reviewers for their constructive comments and suggestions for the improvement of the present research. R.S expresses gratitude to SRM Institute of Science and Technology, Kattankulathur, Chennai, India, for providing financial support for this work. S.B. acknowledges the financial support provided by the National Science and Technology Council of Taiwan (Projects No. 111-2221-E-002-057-MY3 and No. 113-2811-E-002-013-MY2). N.P. gratefully acknowledges financial support from the Irish Research Council (Project No. GOIPD/2024/226).

[1] B. H. Weigl, R. L. Bardell, and C. R. Cabrera, Lab-on-a-chip for drug development, Adv. Drug Deliv. Rev. **55**, 349 (2003).

[2] B. Sharma and A. Sharma, Microfluidics: Recent advances toward lab-on-chip applications in bioanalysis, Adv. Eng. Mater. **24**, 2100738 (2022).

[3] S. Preetam, B. K. Nahak, S. Patra, D. C. Toncu, S. Park, M. Syväjärvi, G. Orive, and A. Tiwari, Emergence of microfluidics for next generation biomedical devices, Biosens. Bioelectron. **10**, 100106 (2022).

[4] B. Boussaha, M. Lahmar, B. Bou-Said, and H. Boucherit, Non-Newtonian couple-stress squeeze film behaviour between oscillating anisotropic porous circular discs with sealed boundary, Mech. Ind. **21**, 311 (2020).

[5] S. Maiti and J. C. Misra, Peristaltic transport of a couple stress fluid: Some applications to hemodynamics, J. Mech. Med. Biol. **12**, 1250048 (2012).

[6] K. Valanis and C. T. Sun, Poiseuille flow of a fluid with couple stress with applications to blood flow, Biorheology **6**, 85 (1969).

[7] G. I. Taylor, Dispersion of soluble matter in solvent flowing slowly through a tube, Proc. R. Soc. A **219**, 186 (1953).

[8] R. Aris, On the dispersion of a solute in a fluid flowing through a tube, Proc. R. Soc. A **235**, 67 (1956).

[9] W. N. Gill and R. Sankarasubramanian, Exact analysis of unsteady convective diffusion, Proc. R. Soc. A **316**, 341 (1970).

[10] P. C. Chatwin, The approach to normality of the concentration distribution of a solute in a solvent flowing along a straight pipe, J. Fluid Mech. **43**, 321 (1970).

[11] N. G. Barton, On the method of moments for solute dispersion, J. Fluid Mech. **126**, 205 (1983).

[12] P. Wang and G. Q. Chen, Solute dispersion in open channel flow with bed absorption, J. Hydrol. **543**, 208 (2016).

[13] V. K. Stokes, Couple stresses in fluids, Phys. Fluids **9**, 1709 (1966).

[14] V. K. Stokes, Couple stresses in fluids, *Theories of Fluids with Microstructure: An Introduction* (Springer, New York, 1984), p. 34.

[15] M. Devakar and T. K. V. K. V. Iyengar, Run up flow of a couple stress fluid between parallel plates, Nonlinear Anal.-Model. Control **15**, 29 (2010).

[16] E. F. El Shehawey and K. S. Mekheimer, Couple-stresses in peristaltic transport of fluids, J. Phys. D **27**, 1163 (1994).

[17] J. R. Lin and C. R. Hung, Combined effects of non-Newtonian couple stresses and fluid inertia on the squeeze film characteristics between a long cylinder and an infinite plate, Fluid Dyn. Res. **39**, 616 (2007).

[18] V. Sharma and S. Kumar, Velocity dispersion in an elastic plate with microstructure: Effects of characteristic length in a couple stress model, Meccanica **49**, 1083 (2014).

[19] G. Radhakrishnamacharya and H. Alemayehu, Dispersion of a solute in peristaltic motion of a couple stress fluid through a porous medium, Tamkang J. Math. **43**, 541 (2012).

[20] V. M. Soundalgekar, Effects of couple stresses in fluids on dispersion of a solute in a channel flow, Phys. Fluids **14**, 19 (1971).

[21] V. M. Soundalgekar, Effects of couple stresses in fluids on the dispersion of a soluble matter in a channel flow with homogeneous and heterogeneous reactions, Int. J. Heat Mass Transf. **18**, 527 (1975).
[22] V. M. Soundalgekar and P. Chaturani, Effects of couple-stresses on the dispersion of a soluble matter in a pipe flow of blood, Rheol Acta **19**, 710 (1980).
[23] N. Rudraiah, D. Pal, and P. G. Siddheshwar, Effect of couple stresses on the unsteady convective diffusion in fluid flow through a channel, Biorheology **23**, 349 (1986).
[24] S. Katz, Chemical reactions catalysed on a tube wall, Chem. Eng. Sci. **10**, 202 (1959).
[25] R. E. Walker, Chemical reaction and diffusion in a catalytic tubular reactor, Phys. Fluids **4**, 1211 (1961).
[26] P. S. Gupta and A. S. Gupta, Effect of homogeneous and heterogeneous reactions on the dispersion of a solute in the laminar flow between two plates, Proc. R. Soc. A **330**, 59 (1972).
[27] W. B. Neely, G. E. Blau, and T. Alfrey, Mathematical models predict concentration-time profiles resulting from chemical spill in a river, Environ. Sci. Technol. **10**, 72 (1976).
[28] D. Philip and P. Chandra, Effects of heterogeneous and homogeneous reactions on the dispersion of a solute in simple micro fluid, Indian J. Pure Appl. Math. **24**, 551 (1993).
[29] C. O. Ng and N. Rudraiah, Convective diffusion in steady flow through a tube with a retentive and absorptive wall, Phys. Fluids **20**, 073604 (2008).
[30] S. Debnath, A. K. Saha, B. S. Mazumder, and A. K. Roy, Transport of a reactive solute in a pulsatile non-Newtonian liquid flowing through an annular pipe, J. Eng. Math. **116**, 1 (2019).
[31] A. K. Roy, A. K. Saha, and S. Debnath, Hydrodynamic dispersion of solute under homogeneous and heterogeneous reactions, Int. J. Heat Technol. **37**, 387 (2019).
[32] W. Jiang and G. Chen, Solute transport in two-zone packed tube flow: Long-time asymptotic expansion, Phys. Fluids **31**, 043303 (2019).
[33] G. Saha, N. Poddar, S. Dhar, B. Mazumder, and K. K. Mondal, Solute dispersion phenomena in a free and forced convective flow with boundary reactions, Eur. J. Mech. B Fluids **100**, 101 (2023).
[34] N. Poddar, D. Das, S. Dhar, and K. K. Mondal, On scalar transport in an oscillatory Couette–Poiseuille flow under the effects of heterogeneous and bulk chemical reactions: A multi-scale approach, Phys. Fluids **35**, 043617 (2023).
[35] C. C. Mei and B. Vernescu, *Homogenization Methods for Multiscale Mechanics* (World Scientific, Singapore, 2010).
[36] C. O. Ng, Dispersion in open-channel flow subject to the processes of sorptive exchange on the bottom and air-water exchange on the free surface, Fluid Dyn. Res. **38**, 359 (2006).
[37] C. O. Ng, Dispersion in steady and oscillatory flows through a tube with reversible and irreversible wall reactions, Proc. R. Soc. A **462**, 481 (2006).
[38] Z. Wu and G. Q. Chen, Analytical solution for scalar transport in open channel flow: Slow-decaying transient effect, J. Hydrol. **519**, 1974 (2014).
[39] Z. Wu and G. Q. Chen, Approach to transverse uniformity of concentration distribution of a solute in a solvent flowing along a straight pipe, J. Fluid Mech. **740**, 196 (2014).
[40] S. Barik and D. C. Dalal, Transverse concentration distribution in an open channel flow with bed absorption: A multi-scale approach, Commun. Nonlinear Sci. Numer. Simul. **65**, 1 (2018).
[41] N. Poddar, S. Dhar, B. S. Mazumder, and K. K. Mondal, An exact analysis of scalar transport in hydromagnetic flow between two parallel plates: A multi-scale approach, Proc. R. Soc. A **477**, 20200830 (2021).
[42] N. Poddar, G. Saha, S. Dhar, and K. K. Mondal, On solute dispersion in an oscillatory magneto-hydrodynamics porous medium flow under the effect of heterogeneous and bulk chemical reaction, Phys. Fluids **34**, 093603 (2022).
[43] S. Dhar, N. Poddar, K. K. Mondal, and B. S. Mazumder, On dispersion of solute in a hydromagnetic flow between two parallel plates with boundary absorption, Phys. Fluids **33**, 083609 (2021).
[44] T. Karmakar, S. Barik, and G. P. Raja Sekhar, Multi-scale analysis of concentration distribution in unsteady Couette–Poiseuille flows through a porous channel, Proc. R. Soc. A **479**, 20220494 (2023).
[45] N. Poddar and P. Wang, Transport of reactive contaminant in a wetland flow with the effects of reversible and irreversible reactions on the bed surface, Int. Commun. Heat Mass Transf. **157**, 107709 (2024).

[46] C. O. Ng and T. L. Yip, Effects of kinetic sorptive exchange on solute transport in open-channel flow, J. Fluid Mech. **446**, 321 (2001).
[47] N. Poddar, G. Saha, K. K. Mondal, S. Dhar, and B. S. Mazumder, Effect of phase exchange kinetics on Taylor dispersion of chemically reactive solutes in an oscillatory magnetohydrodynamics flow between two parallel plates, Phys. Fluids **36**, 053601 (2024).
[48] H. Wang, Z. Wu, J. Zhang, W. Wang, and W. Chen, Analysis of contaminant dispersion in constructed wetland flows with absorptive boundaries, Ecol. Indic. **166**, 112275 (2024).
[49] Aruna A and S. Barik, Multi-scale analysis of solute dispersion in non-Newtonian flows in a tube with wall absorption, Phys. Fluids **35**, 033103 (2023).
[50] Aruna A, S. Barik, and N. Poddar, Transport of a solute in primary and secondary flows through a rotating channel with an absorbing wall, Phys. Fluids **36**, 126629 (2024).
[51] Aruna A, S. Barik, T. Karmakar, and G. P. Raja Sekhar, Multi-scale analysis of solute transport in hydrodynamic fluid flows through a porous channel with anisotropic permeability and boundary absorption, J. Eng. Math. **150**, 3 (2025).
[52] D. Das, N. Poddar, S. Dhar, R. R. Kairi, and K. K. Mondal, Multi-scale approach to analyze the dispersion of solute under the influence of homogeneous and inhomogeneous reactions through a channel, Int. Commun. Heat Mass Transf. **129**, 105709 (2021).
[53] J. C. Umavathi, A. J. Chamkha, M. H. Manjula, and A. Al-Mudhaf, Flow and heat transfer of a couple-stress fluid sandwiched between viscous fluid layers, Can. J. Phys. **83**, 705 (2005).
[54] C. C. Mei, J. L. Auriault, and C.-O. Ng, Some applications of the homogenization theory, Adv. Appl. Mech. **32**, 277 (1996).
[55] P. C. Fife and K. R. K. Nicholes, Dispersion in flow through small tubes, Proc. R. Soc. A **344**, 131 (1975).
[56] S. Radha, S. Barik, and N. Poddar, Transport of pollutant in a channel flow under the influence of homogeneous and inhomogeneous reactions, Commun. Nonlinear Sci. Numer. Simul. **132**, 107892 (2024).
[57] See Supplemental Material http://link.aps.org/supplemental/10.1103/PhysRevFluids.10.014502 for the second- and third-order transverse functions.
[58] M. Devakar, D. Sreenivasu, and B. Shankar, Analytical solutions of couple stress fluid flows with slip boundary conditions, Alex. Eng. J. **53**, 723 (2014).
[59] P. Wang and G. Q. Chen, Transverse concentration distribution in Taylor dispersion: Gill's method of series expansion supported by concentration moments, Int. J. Heat Mass Transf. **95**, 131 (2016).
[60] A. Enders, A. Grünberger, and J. Bahnemann, Towards small scale: Overview and applications of microfluidics in biotechnology, Mol. Biotechnol. **66**, 365 (2024).
[61] S. Barik and D. C. Dalal, Analytical solution for concentration distribution in an open channel flow with phase exchange kinetics, Acta Mech. Sin. **38**, 321506 (2022).
[62] M. Ishaq, S. U. Rehman, M. B. Riaz, and M. Zahid, Hydrodynamical study of couple stress fluid flow in a linearly permeable rectangular channel subject to Darcy porous medium and no-slip boundary conditions, Alex. Eng. J. **91**, 50 (2024).
[63] N. T. M. Eldabe, A. A. Hassan, and M. A. Mohamed, Effect of couple stresses on the MHD of a non-Newtonian unsteady flow between two parallel porous plates, Z. Naturforsch. A **58**, 204 (2003).